Highlights

Spatially-Dependent Model for Rods and Cones in the Retina

Daniel M. Anderson, Danielle C. Brager, Anthony J. Kearsley

- Photoreceptor density linked to rod and cone outer segment length dynamics
- Numerical optimization algorithm links mathematical model with retinal data
- Rod/cone outer segment predictions consistent with spatial and temporal retinal data

Spatially-Dependent Model for Rods and Cones in the Retina

Daniel M. Anderson[a,b], Danielle C. Brager[a,*], Anthony J. Kearsley[a,**]

[a] *Applied & Computational Mathematics Division, National Institute of Standards and Technology, 100 Bureau Drive, Gaithersburg, 20899, Maryland, USA*
[b] *Department of Mathematical Sciences, George Mason University, 4400 University Drive, Fairfax, 22030, Virginia, USA*

Abstract

We develop a mathematical model for photoreceptors in the retina. We focus on rod and cone outer segment dynamics and interactions with a nutrient source associated with the retinal pigment epithelium cells. Rod and cone densities (number per unit area of retinal surface) are known to have significant spatial dependence in the retina with cones located primarily near the fovea and the rods located primarily away from the fovea. Our model accounts for this spatial dependence of the rod and cone photoreceptor density as well as for the possibility of nutrient diffusion. We present equilibrium and dynamic solutions, discuss their relation to existing models, and estimate model parameters through comparisons with available experimental measurements of both spatial and temporal photoreceptor characteristics. Our model compares well with existing data on spatially-dependent regrowth of photoreceptor outer segments in the macular region of Rhesus Monkeys. Our predictions are also consistent with existing data on the spatial dependence of photoreceptor outer segment length near the fovea in healthy human subjects. We focus primarily on the healthy eye but our model could be the basis for future efforts designed to explore various retinal pathologies, eye-related injuries, and treatments of these conditions.

*Present Address: NASDAQ
**Corresponding Author
Email addresses: daniel.anderson@nist.gov (Daniel M. Anderson), dcbrager@gmail.com (Danielle C. Brager), anthony.kearsley@nist.gov (Anthony J. Kearsley)

Keywords: Photoreceptor, Rods, Cones, Retina, Mathematical Model

1. Introduction

The light reflected into your eyes from the colorful, sun-lit plumage of a scarlet macaw, or from a fast-moving car in your peripheral view, or from a dimly-lit obstacle in your path on a dark, moonless night is processed by your brain in a figurative 'blink of an eye'. The light's path through this complex optical system – the outermost tear film, cornea, anterior chamber, pupil, lens, and vitreous chamber – results in focused light into the retina, which is the thin, light-sensitive tissue at the back of the eye that converts light into electrochemical signals sent on to the brain via the optic nerve resulting in, for healthy eyes, visual recognition. The retina itself has a multitude of components and functions (e.g. see Fatt & Weissman [23], Roberts *et al.* [52]) but for the purposes of the present study we view the retina as composed of two types of photoreceptors – rods and cones – and an underlying retinal pigment epithelium (RPE). Rods are known to be responsible for visual function in low-light (night vision) and peripheral vision. Cones are responsible for day vision, color vision, and visual acuity. A photoreceptor includes an inner segment (IS) and an outer segment (OS). The photoreceptor IS, as the main site of the mitochondria, is the photoreceptor's metabolic center. The photoreceptor's OS is made up of disc-like lamellae and contain photopigments that absorb incident photons and undergo structural alteration in the process of creating electrochemical signals. The outer segments (of length on the order of 30 μm to 50 μm in human photoreceptors [67]) undergo continuous shedding and periodic renewal facilitated by the RPE [6] which acts to recycle the shed parts of the OS and serves as an effective nutrient source sustaining the function of the rods and cones [3, 62].

The organization and distribution of rods and cones in the retina – the photoreceptor mosaic [3] – varies across species. For humans the cone density is maximum

in the fovea – a small depression in the central, macular region, of the retina – and diminishes rapidly away from this region. The rods have effectively zero density near the fovea, reach a maximum density at an intermediate distance from the fovea, and have a density that diminishes slowly as the ora serrata – the photosensitive limit of the retina boundary – is approached. Curcio *et al.* [21] reported thorough measurements of the photoreceptor mosaic on whole-mounted human retinas that revealed the photoreceptor structure and characteristics described above. More recently, highly sophisticated imaging techniques such as Adaptive Optics Scanning Laser Ophthalmoscope (AOSLO) [16, 17, 19, 20, 30, 36, 45, 57, 61, 64, 65, 67], related Adaptive Optics (AO)-based methods [33, 39] and other non-AO techniques [40] have been used to obtain high resolution *in vivo* measurements of rod and/or cone photoreceptor density and structure across the retina. Related techniques have also been used to image the RPE mosaic [55] and the photoreceptor inner segment structure [58]. Various studies (e.g. Mehri [43]) have explored mathematically fitting the photoreceptor density data in various directions from the fovea (e.g. nasal, temporal, superior, inferior). In the present study we characterize the rod and cone densities with mathematical functions used in Roberts *et al.* [53] (further details are given in the next section).

Other specialized imaging methods such as Optical Coherence Tomography (OCT) have been used to probe details of retinal layer structure and depth. The study of Wilk *et al.* [67], for example, reported measurements of human photoreceptor OS lengths at different positions across the retina especially in the region near the fovea (e.g. see their Table 1 and their OCT images in Figures 1, 2, and 3). Other related studies reporting measurements of human OS lengths as functions of position in the retina include Cakir *et al.* [9] (see their Figure 2 and Table 2) and Domdei *et al.* [22] (see their Figures 5 and 6). We shall make direct use of the Wilk *et al.* data in comparison to our model predictions for spatial dependence of OS lengths. Others (e.g. Kafieh *et al.* [31], Liu *et al.* [38], and Menghini *et al.* [44]) have reported OS length variation with position

in the retina along with thickness information about other retinal layers (inner and outer nuclear layers, inner and outer segments, RPE, etc.). Maden *et al.* [41] reported measurements of the human OS length at the fovea center that showed this value to be fairly uniform (roughly 50 μm to 60 μm) for a healthy population across a broad range of ages up to 60 years and as well as with respect to gender. Recent studies by Reumueller *et al.* [48, 49] have combined AO and OCT techniques to explore the three-dimensional structure of photoreceptor densities at different layers in the retina.

There are a number of retinal diseases, among them macular degeneration and retinitis pigmentosa (e.g. [63, 68]), as well as other types of damage or injuries such as retinal tear and/or detachment and damage due to radiant exposure (e.g. [42]). In the present work we do not focus on issues specific to retinal diseases and injuries, but recognize that these have motivated much eye-related research including many efforts in mathematical modeling of the retina. Several of these mathematical models have inspired our work and we outline these below.

Mathematical models that have been directed towards an improved understanding of retinitis pigmentosa (RP), for example, include those of Camacho and coworkers (e.g. [10, 11, 14, 15]). These models have been formulated as systems of ordinary differential equations for dynamic variables representing cumulative photoreceptor populations and a nutrient supply. In Camacho *et al.* [10], for example, coupled ODEs for three variables – representing rod, cone, and nutrient quantities in a healthy eye – were written down that account for rod and cone shedding and renewal processes, nutrient supply, consumption of nutrient by rods and cones, as well as a rod-cone interaction known as the rod-derived cone viability factor (RdCVF) which accounts for the presence of a rod-generated protein that aids in the survival of cones (e.g. [10, 12, 35]). Camacho & coworkers [14, 15] developed and analyzed an extension of the Camacho *et al.* [10] model to account for the presence of two different rod populations – normal rods and mutated rods – and to explore the association of RP with the presence of

rods with gene mutations. This model was later used to ask questions about optimal control and treatment strategies for diseases such as RP [11, 13].

Other mathematical models have asked different questions about photoreceptor dynamics from a pattern formation point of view. Models such as those by Burns *et al.* [8], Shoaf *et al.* [59], and Conway [18] formulate reaction-diffusion (partial differential equation) models. These tend to be in the spirit of biological morphogenesis such as the Gierer–Meinhardt system [26] and mathematical and computational analyses thereof (e.g. [25]).

A collection of work that addresses various aspects of spatio-temporal dynamics of retinal processes also with a view towards improved understanding of retinal diseases such as RP is that of Roberts and coworkers [50, 51, 52, 53, 54]. One of these – Roberts *et al.* [52] – provides an excellent and comprehensive review of the state of theoretical modeling of the retina and related pathologies.

Roberts *et al.* [53] investigated the 'oxygen toxicity hypothesis' (one of four main hypothesis believed to be important for the understanding of RP – the other three being the 'trophic factor hypothesis', the 'toxic substance hypothesis', and the 'microglia hypothesis'). In their model, Roberts *et al.* introduced an oxygen concentration variable that depended on the spatial position in the retina (an angle measure from the fovea) and time. They posed a partial differential equation that accounted for oxygen diffusion as well as uptake of oxygen and exchange with the capillary bed of the choroid layer of the retina. This reaction diffusion equation was coupled to a photoreceptor dynamics equation that involved a regrowth term accounting for the spatial dependence of the photoreceptor density (using photoreceptor density measurements of Curcio *et al.* [21]) as well as a capillary dynamics equation that also incorporated photoreceptor spatial structure. With this model they examined spatio-temporal dynamics of degenerate patches of retina as well as the response of the retina to treatment. In a related study, Roberts *et al.* [54] explored these spatio-temporal dynamics in a two-dimensional

domain representing the entire retina including the possibility of mutation-induced rod and cone degeneration, first explored in their earlier work [53].

In another study Roberts *et al.* [51] explored the 'trophic factor hypothesis' in the context of a retina model for RP. In this model a spatially-dependent diffusible trophic substance was modeled by a reaction diffusion equation in which the substance was produced in proportion to the local rod density, consumed in proportion to the local cone density and was subject to decay and treatment modalities. Various models for rod and/or cone degeneration, which would impact the local rod and/or cone densities were also incorporated. In the case where cone regeneration was included a model was posed also for the local cone OS length. Predictions were given related to the dynamics and prevention of cone degeneration driven by the trophic factor mechanisms. These spatio-temporal dynamics were further explored in a related context by Roberts [50].

The models of Roberts *et al.* [51, 53] have a number of similarities with the model we develop in the present work. Specifically, as outlined in more detail below, we also incorporate both diffusion – in our case a nutrient consumed by both rods and cones – and spatial dependence of rod and cone densities (photoreceptors per unit area of retina). As described below, our model will also connect closely with ideas from the Camacho & Wirkus [15] model.

In the present work we derive a model to describe the dynamics of rod OS and cone OS lengths as a function of position in the retina. We focus on a one-dimensional problem where spatial position in the retina is measured by an angle θ from the fovea towards the outer periphery (ora serrata) of the retina. We introduce variables $r(\theta, t)$ and $c(\theta, t)$ to represent the rod and cone OS lengths at location θ and time t while the variable $T(\theta, t)$ represents the local nutrient concentration (molarity, in M or mol per liter). We also introduce functions $R(\theta)$ and $C(\theta)$ that represent the rod and cone densities (i.e. number of rods per unit area and number of cones per unit area) whose spatial dependence has been measured for human subjects (e.g. [21]) as well as for

primates (e.g. [2, 4, 24, 34, 66]), among other species (e.g. [56]). In our model the densities R and C will be assumed given – consistent with experimental measurements – and independent of time. In general, the retinal pigment epithelium (RPE) cells also have a spatially-dependent density (e.g. see [1, 5, 7, 27, 37, 47, 60]) but we do not incorporate that feature of the RPE into our model.

The nutrient is assumed to be consumed by rods and cones and replenishes itself locally by a self-regulating mechanism. Our model has been inspired in part by the Camacho & Wirkus [15] model developed for rod, cone, and nutrient dynamics in the retina but adapted to include spatial dependence of the rod and cone densities as well as the diffusion of nutrient. Specifically, to provide context for our model we revisit the Healthy Eye Model by Camacho & Wirkus [15], defined by their equations (1), which is given by

$$\frac{d\mathcal{R}_n^{\mathrm{CW}}}{dt} = \mathcal{R}_n^{\mathrm{CW}}(a_n^{\mathrm{CW}}\mathcal{T}^{\mathrm{CW}} - \mu_n^{\mathrm{CW}}), \tag{1}$$

$$\frac{d\mathcal{C}^{\mathrm{CW}}}{dt} = \mathcal{C}^{\mathrm{CW}}(a_c^{\mathrm{CW}}\mathcal{T}^{\mathrm{CW}} - \mu_c^{\mathrm{CW}} + d_n^{\mathrm{CW}}\mathcal{R}_n^{\mathrm{CW}}), \tag{2}$$

$$\frac{d\mathcal{T}^{\mathrm{CW}}}{dt} = \mathcal{T}^{\mathrm{CW}}(\Gamma^{\mathrm{CW}} - \kappa^{\mathrm{CW}}\mathcal{T}^{\mathrm{CW}} - \beta_n^{\mathrm{CW}}\mathcal{R}_n^{\mathrm{CW}} - \gamma^{\mathrm{CW}}\mathcal{C}^{\mathrm{CW}}). \tag{3}$$

Here $\mathcal{R}_n^{\mathrm{CW}}$ and $\mathcal{C}^{\mathrm{CW}}$ represent the number of rod OS and cone OS, respectively, and $\mathcal{T}^{\mathrm{CW}}$ represents the total number of retinal pigment epithelium (RPE) cells. The parameters appearing here represent the rate constants associated with consumption of the nutrient by the rods (a_n^{CW}; units: day^{-1} RPE^{-1}) and by the cones (a_c^{CW}; units: day^{-1} RPE^{-1}), the rate constants associated with rod OS shedding (μ_n^{CW}; units: day^{-1}) and cone OS shedding (μ_c^{CW}; units: day^{-1}), the constant per-cell rate at which rods help cones via the RdCVF effect (d_n^{CW}; units: day^{-1} Rod OS^{-1}), the total inflow rate into the trophic pool (Γ^{CW}; units: day^{-1}), the limiting capacity of trophic factors (κ^{CW}; units: day^{-1} RPE^{-1}), and the rate constants associated with removal of nutrients by rods (β_n^{CW}; units: day^{-1} Rod OS^{-1}) and by cones (γ^{CW}; units: day^{-1} Cone OS^{-1}). This model accounts for temporal dynamics of cumulative variables for rods, cones, and

nutrient but does not attempt to resolve any spatial dependence of these quantities. Camacho & Wirkus point out that their "model does not make the distinction, for example, between 10 rods at half their normal height and 5 rods at their normal height." While our model follows in the spirit of theirs, we have the specific objective of making the distinction between rod and cone OS lengths and rod and cone densities. We emphasize that both photoreceptor OS lengths and photoreceptor densities are known to vary considerably across the retina (e.g. Wilk *et al.* [67] for OS variation and Curcio *et al.* [21] for photoreceptor density variation). Values for the various parameters appearing in equations (1)–(3) were identified by Camacho & Wirkus [15] (see their Table 1) in their comparison to experimental data by Guérin *et al.* [28, 29]. In the context of our model, we shall also make comparisons to the Guérin *et al.* data.

Our paper is organized as follows. In Section 2 we present the derivation of our model for the spatial–temporal dynamics of rod and cone OS lengths as well as the nutrient concentration. In Section 3 we analyze details of equilibrium solutions of interest. In Section 4 we identify connections of our model to the Camacho & Wirkus [15] model. In Section 5 we revisit the Rhesus Monkey retinal reattachment and OS growth data of Guérin *et al.* [28, 29] and show how our model compares with their measurements. In Section 6 we compare our model predictions to a set of measurements reported by Wilk *et al.* [67] on spatial dependence of healthy human photoreceptor OS lengths. Finally, in Section 7 we give conclusions. The appendix includes various data on Rhesus Monkey photoreceptor density measurements obtained from Adams *et al.* [2] as well as human photoreceptor OS length data extracted from images in Wilk *et al.* [67].

2. Model Derivation

Consider a small sample, or *parcel*, of the retina that, in the spirit of a continuum mechanics description (e.g. see the discussion in [52]), can be considered both infinitesimally small – so that it is associated with a particular location in the retina – and

simultaneously contains a sufficiently large number of rods and cones – so that rod and cone densities (per unit area of retina) can be defined for that particular location. For each such parcel (i.e. at each location in the retina) we also assume that we can define average rod and cone OS lengths. Within this basic framework, we shall use conservation arguments applied to such a parcel to generate a set of governing equations. We formulate the basic equations first in two dimensions corresponding to the surface of the retina but later focus our analysis and computations in one-dimensional settings.

2.1. Rod OS Length Evolution

The total rod OS length associated with a given location in the retina is the average rod OS length r times the local rod density R (units: Rod OS m^{-2}) times an area ΔA

$$\text{Total Rod OS Length} \;=\; rR\Delta A. \tag{4}$$

We postulate a basic balance law for rod OS length evolution given by

$$\begin{aligned}\frac{\partial}{\partial t}\,(\text{Total Rod OS Length}) \;=\;& \text{Rate of Rod OS growth stimulated by nutrient}\\ &- \text{Rate of Rod OS shedding.}\end{aligned} \tag{5}$$

We model the rate of rod OS growth stimulated by the nutrient by

$$\text{Rate of Rod OS growth stimulated by nutrient} \;=\; a_r^*(\ell_r - r)TrR\Delta A, \tag{6}$$

where a_r^* is a rate constant (units: M^{-1} m^{-1} s^{-1}) associated with consumption of the nutrient by the rods and ℓ_r is a length scale. That is, the rate of generation of local rod OS length is proportional to the local nutrient concentration, T, and the total (but local) rod OS length ($rR\Delta A$) with a rod length dependent logistic factor $a_r^*(\ell_r - r)$. That the growth is proportional to rod length mimics on the local scale the cumulative variable formulation of Camacho & Wirkus [15]. Other models for growth are also possible (see Roberts [51], equation (4)). The quantity ℓ_r has the interpretation that it is the maximum attainable rod OS length in the absence of other influences (e.g. such as

rod OS shedding). In the next section, we will show how ℓ_r is related to the equilibrium rod OS length. In principle, the quantity ℓ_r could be dependent on location across the retina, perhaps in some way related to the overall retinal thickness which is known to vary across the retina [32], but in the present work we assume it to be a constant.

We model the rate of rod OS shedding by

$$\text{Rate of Rod OS shedding} \;=\; \mu_r^* r R \Delta A, \tag{7}$$

where μ_r^* is a rate constant (units: s^{-1}) associated with shedding.

Putting these together gives

$$\frac{\partial}{\partial t}\left(rR\Delta A\right) \;=\; a_r^* T(\ell_r - r) rR\Delta A - \mu_r^* rR\Delta A. \tag{8}$$

With the assumption that the local rod density, R, is independent of time we find that the local rod OS length satisfies

$$\frac{\partial r}{\partial t} \;=\; r\Big[a_r^*(\ell_r - r)T - \mu_r^*\Big]. \tag{9}$$

Although no spatial derivatives appear in this equation, we note that both r and T depend on space and time. We also remark that when $\ell_r \gg r$ this equation has the approximate growth rate factor $a_r^*\ell_r$ and would match the result of making the substitution $\mathcal{R}_n^{\mathrm{CW}} \to Rr\Delta A$ and $\mathcal{T}^{\mathrm{CW}} \to T$ in the Camacho & Wirkus equation (1).

2.2. Cone OS Length Evolution

Similarly to the rods in (4), the total cone OS length at a given location is the average cone OS length c times the local cone density C (units: Cone OS m^{-2}) times the area ΔA

$$\text{Total Cone OS Length} \;=\; cC\Delta A. \tag{10}$$

We postulate a basic balance law for cone OS length evolution given by

$$\begin{aligned}\frac{\partial}{\partial t}\left(\text{Total Cone OS Length}\right) \;=\;& \text{Rate of OS growth stimulated by nutrient}\\ &+ \text{Rate of Cone OS growth stimulated by Rods}\\ &- \text{Rate of Cone OS shedding.}\end{aligned} \tag{11}$$

The rate of cone OS growth stimulated by the nutrient is similar to that for rods

$$\text{Rate of Cone OS growth stimulated by nutrient} \;=\; a_c^*(\ell_c - c)TcC\Delta A, \quad (12)$$

where a_c^* is a rate constant (units: $\mathrm{M}^{-1}\ \mathrm{m}^{-1}\ \mathrm{s}^{-1}$) associated with consumption of the nutrient by the cones and ℓ_c is a cone-related length scale analogous to ℓ_r.

We assume, as in Camacho & Wirkus [15], that the cones benefit from the proximity of rods (via RdCVF). We model this by

$$\text{Rate of Cone OS growth stimulated by rods} \;=\; d^*(\ell_c - c)\Big[rR\Delta A\Big]cC\Delta A, \quad (13)$$

where d^* is a rate constant (units: Rod $\mathrm{OS}^{-1}\ \mathrm{m}^{-2}\ \mathrm{s}^{-1}$) associated with RdCVF. Note that this term takes the same form as the cone OS growth via the nutrient except that the nutrient factor a_c^*T is replaced by the factor $d^*rR\Delta A$.

The rate of cone OS shedding is

$$\text{Rate of Cone OS shedding} \;=\; \mu_c^* cC\Delta A, \quad (14)$$

where μ_c^* is a rate constant (units: s^{-1}) associated with shedding.

Putting these together gives

$$\frac{\partial}{\partial t}(cC\Delta A) \;=\; a_c^*T(\ell_c - c)cC\Delta A + d^*(\ell_c - c)\Big[rR\Delta A\Big]\Big[cC\Delta A\Big] - \mu_c^* cC\Delta A. \quad (15)$$

As was the case for rods, we shall assume that the local cone density C varies with position in the retina but is not a function of time. Therefore, cancelling common terms gives

$$\frac{\partial c}{\partial t} \;=\; c\Big[a_c^*(\ell_c - c)T + d^*(\ell_c - c)\Big(rR\Delta A\Big) - \mu_c^*\Big]. \quad (16)$$

We note that the factor $d^*\Delta A$ appears, which may suggest it to be negligible as a direct source of cone growth in this model. That said, to retain the RdCVF term as an explicit effect in the cone length evolution equation, we shall for now assume that the factor $d^*\Delta A$ remains $\mathcal{O}(1)$ as $\Delta A \to 0$.

2.3. Nutrient (Trophic Pool) Evolution

The total quantity of nutrient available in a representative volume, ΔV, associated with the RPE is

$$\text{Total Nutrient} \;=\; T\Delta V \tag{17}$$

where T is a nutrient concentration (units: M).

We postulate a basic balance law for nutrient evolution given by

$$\begin{aligned}\frac{\partial}{\partial t}(\text{Total Nutrient}) \;=\;& \text{Self Regulation up to some carrying capacity}\\ &- \text{Consumption by Rods} - \text{Consumption by Cones}\\ &+ \text{Transport by Diffusion.}\end{aligned} \tag{18}$$

The self regulation/carrying capacity term is

$$T(\Gamma^* - \kappa^* T)\Delta V, \tag{19}$$

where Γ^* (units: s^{-1}) and κ^* (units: $\mathrm{s}^{-1}\ \mathrm{M}^{-1}$) are constants. This matches the form for cumulative RPE cells in Camacho & Wirkus [15] with a maximum nutrient carrying capacity of Γ^*/κ^*. In the absence of consumption by rods and cones this form effectively sets the upper limit on the nutrient level.

The consumption by rods and cones have the forms

$$\text{Consumption by Rods} \;=\; \beta^*(\ell_r - r)TrR\Delta V, \tag{20}$$

$$\text{Consumption by Cones} \;=\; \gamma^*(\ell_c - c)TcC\Delta V, \tag{21}$$

where β^* (units: Rod $\mathrm{OS}^{-1}\ \mathrm{s}^{-1}$) and γ^* (units: Cone $\mathrm{OS}^{-1}\ \mathrm{s}^{-1}$) are constants.

The transport via diffusive flux out of the control volume ΔV has the form

$$\text{Transport by Diffusion} = -\nabla\cdot(-D^*\nabla T)\Delta V, \tag{22}$$

where $-D^*\nabla T$ is the standard form for the Fickian flux with diffusion coefficient D^* (units: $\mathrm{m}^2\ \mathrm{s}^{-1}$). We shall later consider diffusion in one dimension measured by angle θ across the retina in which case this takes the form examined by Roberts (e.g. [51, 53])

$$\text{Transport by Diffusion} = \frac{D^*}{R_{retina}^2 \sin\theta} \frac{\partial}{\partial\theta}\left(\sin\theta \frac{\partial T}{\partial\theta}\right)\Delta V, \tag{23}$$

where R_{retina} is the radial position of the retina.

Putting these together and cancelling the common factor ΔV gives

$$\frac{\partial T}{\partial t} = T\Big(\Gamma^* - \kappa^* T - \beta^*(\ell_r - r)rR - \gamma^*(\ell_c - c)cC\Big) + \nabla\cdot(D^*\nabla T). \tag{24}$$

With or without the diffusion term, this equation has spatial dependence through the rod and cone density functions R and C. That is, consumption of nutrient by rods and cones comes in proportion to the local rod and cone densities.

2.4. Model Nondimensionalization

For a one-dimensional section of the retina along an arc parameterized by θ we have

$$\frac{\partial r}{\partial t} = r\Big(a_r^*(\ell_r - r)T - \mu_r^*\Big), \tag{25}$$

$$\frac{\partial c}{\partial t} = c\Big(a_c^*(\ell_c - c)T + d^*\Big[rR\Delta A\Big](\ell_c - c) - \mu_c^*\Big), \tag{26}$$

$$\frac{\partial T}{\partial t} = T\Big(\Gamma^* - \kappa^* T - \beta^*(\ell_r - r)rR - \gamma^*(\ell_c - c)cC\Big) + \frac{D^*}{R_{\text{retina}}^2 \sin\theta}\frac{\partial}{\partial\theta}\left(\sin\theta\frac{\partial T}{\partial\theta}\right). \tag{27}$$

From Roberts *et al.* [53] we take R and C to have the forms

$$R(\theta) = B_3\theta\exp(-b_3\theta), \tag{28}$$

$$C(\theta) = B_1\exp(-b_1\theta) + B_2\exp(-b_2\theta). \tag{29}$$

Roberts [53] gave values for the parameters B_i and b_i based on photoreceptor density data in Curcio *et al.* [21]. We list those values in Table 1 along with another set that we have generated by fitting the same functional forms in equations (28) and (29) to

rod and cone density data for Rhesus Monkeys [2]. Equations (28) and (29) apply over the range $\theta \in [\theta_{\text{fovea}}, \theta_{\text{oraserrata}}]$. Plots of these rod and cone densities for humans and for Rhesus Monkeys are shown in Figure 1.

	Human [21, 53, 67]	Rhesus Monkey [2, 29]	units
B_1	1.73×10^5	0.391×10^5	(OS mm^{-2})
B_2	0.176×10^5	0.121×10^5	(OS mm^{-2})
B_3	8.84×10^5	7.04×10^5	(OS mm^{-2} radian^{-1})
b_1	54.1	24.6	(radian^{-1})
b_2	2.01	1.82	(radian^{-1})
b_3	2.31	2.71	(radian^{-1})
R_{max}	1.41×10^5	0.955×10^5	(OS per mm^2)
C_{max}	1.91×10^5	0.512×10^5	(OS per mm^2)
r_{normal}	55 [67]	29.2 [29]	(μm)
c_{normal}	55 [67]	19.7 [29]	(μm)
θ_{fovea}	0	0	(radians)
$\theta_{\text{oraserrata}}$	1.33	1.02	(radians)
R_{retina}	11.06 [21]	10.71 [2]	(mm)
A_{retina}	585.29	343.79	(mm^2)

Table 1: Fitted parameters used in the rod and cone density functions in equations (28) and (29). The values for the human retina are those reported in Roberts *et al.* [53] based on data by Curcio *et al.* [21]. We obtained the values for the Rhesus Monkey retinas by fitting data in Figure 2 of the paper by Adams *et al.* [2] (see our Table A.7) to equations (28) and (29). Note that in terms of equations (28) and (29), $R_{\text{max}} = B_3/(eb_3)$ and $C_{\text{max}} = B_1 + B_2$. We have assumed that $A_{\text{retina}} = 2\pi R_{\text{retina}}^2(1 - \cos\theta_{\text{oraserrata}})$.

Now, define the dimensionless quantities $\bar{r}$, $\bar{c}$, $\bar{T}$, and $\bar{t}$ as

$$\bar{r} = \frac{r}{r_{\text{normal}}}, \quad \bar{c} = \frac{c}{c_{\text{normal}}}, \quad \bar{T} = \frac{T}{\Gamma^*/\kappa^*}, \quad \bar{t} = \frac{t}{(1/\Gamma^*)}, \tag{30}$$

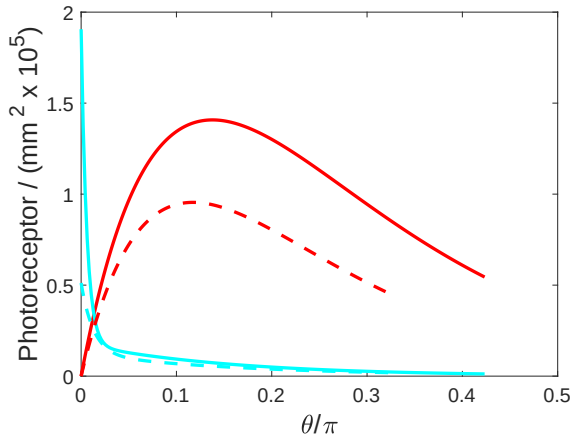

Figure 1: This plot shows the rod and cone densities as a function of θ (distance in radians from the fovea) for a human retina (solid curves) based on data from Curcio *et al.* [21] and Roberts *et al.* [53] and for a Rhesus Monkey retina (dashed curves) based on data from Adams *et al.* [2]. The red lines show the rod densities and the cyan lines show the cone densities. In both cases the curves represent fits using equations (28) and (29) with coefficients as shown in Table 1. Our corresponding estimates for total rod and cone photoreceptors are $\mathcal{N}_R = 5.76 \times 10^7$ and $\mathcal{N}_C = 2.32 \times 10^6$ for the human retina and $\mathcal{N}_R = 2.46 \times 10^7$ and $\mathcal{N}_C = 1.41 \times 10^6$ for the Rhesus Monkey retina.

where r_{normal} and c_{normal} represent normal (healthy) reference values for r and c, respectively, over the entire retina (see Table 1). We also denote

$$\bar{R} = \frac{R}{R_{\max}}, \quad \bar{C} = \frac{C}{C_{\max}}, \quad \bar{\ell}_r = \frac{\ell_r}{r_{\text{normal}}}, \quad \bar{\ell}_c = \frac{\ell_c}{c_{\text{normal}}}, \tag{31}$$

where $R_{\max}$ and $C_{\max}$ are the maximum rod and cone densities defined in Table 1.

Our dimensionless governing equations are

$$\frac{\partial \bar{r}}{\partial \bar{t}} = \bar{r}\Big(a_r(\bar{\ell}_r - \bar{r})\bar{T} - \mu_r\Big), \tag{32}$$

$$\frac{\partial \bar{c}}{\partial \bar{t}} = \bar{c}\Big(a_c(\bar{\ell}_c - \bar{c})\bar{T} + d\bar{r}\bar{R}(\bar{\ell}_c - \bar{c}) - \mu_c\Big), \tag{33}$$

$$\frac{\partial \bar{T}}{\partial \bar{t}} = \bar{T}\Big(1 - \bar{T} - \beta(\bar{\ell}_r - \bar{r})\bar{r}\bar{R} - \gamma(\bar{\ell}_c - \bar{c})\bar{c}\bar{C}\Big) + \frac{D}{\sin\theta}\frac{\partial}{\partial\theta}\left(\sin\theta\frac{\partial \bar{T}}{\partial\theta}\right), \tag{34}$$

subject to initial conditions $\bar{r}(\theta, 0) = \bar{r}_0(\theta)$, $\bar{c}(\theta, 0) = \bar{c}_0(\theta)$, and $\bar{T}(\theta, 0) = \bar{T}_0(\theta)$, where $\bar{r}_0$, $\bar{c}_0$, and $\bar{T}_0$ are initial values for rod OS length, cone OS length, and trophic

pool relative to the scales r_{normal}, c_{normal}, and Γ^*/κ^*, respectively. The dimensionless parameters appearing here are

$$a_r = \frac{a_r^* r_{\text{normal}}}{\kappa^*}, \quad \mu_r = \frac{\mu_r^*}{\Gamma^*}, \quad a_c = \frac{a_c^* c_{\text{normal}}}{\kappa^*}, \quad \mu_c = \frac{\mu_c^*}{\Gamma^*},$$
$$d = \frac{d^* r_{normal} c_{\text{normal}} R_{\max} \Delta A}{\Gamma^*}, \tag{35}$$
$$\beta = \frac{\beta^* (r_{\text{normal}})^2 R_{\max}}{\Gamma^*}, \quad \gamma = \frac{\gamma^* (c_{\text{normal}})^2 C_{\max}}{\Gamma^*}, \quad D = \frac{D^*}{\Gamma^* R_{\text{retina}}^2}.$$

When diffusion is included ($D \neq 0$) we use no-flux boundary conditions ($\partial T/\partial\theta = 0$) at $\theta = \theta_{\text{fovea}}$ and $\theta = \theta_{\text{oraserrata}}$. If diffusion is neglected ($D = 0$) no boundary conditions are needed as the spatial variable θ appears only as a parameter.

3. Equilibria

The equilibrium solutions are determined by equations (32)–(34) with time derivatives set to zero. We denote equilibrium variables, which in general depend on θ, by $\bar{r}_{\text{eq}}$, $\bar{c}_{\text{eq}}$, and $\bar{T}_{\text{eq}}$. There are equilibrium solutions of the following forms:

- Absence of rod OS, cone OS, and nutrient: $\bar{r}_{\text{eq}} = \bar{c}_{\text{eq}} = \bar{T}_{\text{eq}} = 0$.
- Absence of rod OS: $\bar{r}_{\text{eq}} = 0$, $\bar{c}_{\text{eq}} \neq 0$, $\bar{T}_{\text{eq}} \neq 0$.
- Absence of cone OS: $\bar{r}_{\text{eq}} \neq 0$, $\bar{c}_{\text{eq}} = 0$, $\bar{T}_{\text{eq}} \neq 0$.
- Absence of rod OS and cone OS: $\bar{r}_{\text{eq}} = \bar{c}_{\text{eq}} = 0$, $\bar{T}_{\text{eq}} \neq 0$.
- Presence of rod OS, cone OS, and nutrient: $\bar{r}_{\text{eq}} \neq 0$, $\bar{c}_{\text{eq}} \neq 0$, $\bar{T}_{\text{eq}} \neq 0$.

As our focus is on a healthy eye state we shall only discuss the last situation. Assuming that the equilibrium rod OS length is nonzero everywhere, it follows that

$$\bar{r}_{\text{eq}} = \bar{\ell}_r - \frac{p_r}{\bar{T}_{\text{eq}}}, \tag{36}$$

where $p_r = \mu_r/a_r$. This shows that the equilibrium rod length is lower than the value $\bar{\ell}_r$ by a rod OS shedding term inversely proportional to the local nutrient supply $\bar{T}_{eq}$.

Spatial dependence of the rod OS length enters through spatial dependence of the nutrient (see below). Similarly, for the cone OS length we find that

$$\bar{c}_{\rm eq} = \bar{\ell}_c - \frac{p_c}{\bar{T}_{\rm eq} + p_d \bar{r}_{\rm eq} \bar{R}}, \tag{37}$$

where $p_c = \mu_c/a_c$ and $p_d = d/a_c$. This cone OS equilibrium length is similar to that for rods but is modified by an additional factor related to RdCVF in which the rod density appears explicitly. The corresponding equation for $\bar{T}_{\rm eq}$ is given by

$$0 = \bar{T}_{\rm eq}(1 - \bar{T}_{\rm eq}) - \beta p_r \bar{r}_{\rm eq} \bar{R} - \gamma \frac{p_c}{1 + p_d(\bar{r}_{\rm eq}\bar{R}/\bar{T}_{\rm eq})} \bar{c}_{\rm eq} \bar{C} + \frac{D}{\sin\theta} \frac{\partial}{\partial\theta} \left(\sin\theta \frac{\partial \bar{T}_{\rm eq}}{\partial\theta} \right), \tag{38}$$

where $\bar{T}_{\rm eq}$ is subject to boundary conditions $\partial\bar{T}_{\rm eq}/\partial\theta = 0$ at $\theta = \theta_{\rm fovea}$ and at $\theta = \theta_{\rm oraserrata}$ when $D \neq 0$. Both rod and cone densities enter this expression for nutrient distribution. In these equations there are eight relevant parameters/parameter groups

$$p_r \equiv \frac{\mu_r}{a_r}, \quad p_c \equiv \frac{\mu_c}{a_c}, \quad p_d \equiv \frac{d}{a_c}, \quad \beta, \quad \gamma, \quad D, \quad \bar{\ell}_r, \quad \bar{\ell}_c. \tag{39}$$

As we show later, a further reduced set of parameters in which $d = 0$, $\gamma = 0$, and $D = 0$ (giving a five-parameter system, or four with the condition $\bar{\ell}_r = \bar{\ell}_c$, or three if also $p_r = p_c$) allows a good fit to measured photoreceptor OS length data from Wilk *et al.* [67]. If one looks at the equilibrium conditions under the assumption that $D = 0$ (zero diffusion) and if γ is sufficiently small (but also for larger values of γ in regions away from the fovea where the cone density $\bar{C}(\theta) \approx 0$) the trophic nutrient concentration satisfies a cubic equation

$$0 = \bar{T}_{\rm eq} \left[\bar{T}_{\rm eq}^2 - \bar{T}_{\rm eq} + p_r \beta \bar{\ell}_r \bar{R} \right] - p_r^2 \beta \bar{R}. \tag{40}$$

In this case only the parameters p_r, β, and $\bar{\ell}_r$ (along with $\bar{R}$) influence the form of $\bar{T}_{\rm eq}$. Here, $\bar{r}_{\rm eq}$ is still given by equation (36). If the term d is also neglected then $\bar{c}_{\rm eq}$ has a similar form to that of $\bar{r}_{\rm eq}$ given by

$$\bar{c}_{\rm eq} = \bar{\ell}_c - \frac{p_c}{\bar{T}_{\rm eq}}. \tag{41}$$

Under the assumptions outlined, the spatial dependence inherited by $\bar{T}_{\text{eq}}$ and, consequently, $\bar{r}_{\text{eq}}$ and $\bar{c}_{\text{eq}}$, comes exclusively from the θ dependence of rod-density function $\bar{R}(\theta)$. This appears to be the simplest version of our model that allows for photoreceptor OS length spatial dependence in relation to photoreceptor density. The key terms in the model from this perspective are the shedding and renewal of rod OS, shedding and renewal of cone OS, and uptake of nutrient due primarily to consumption by rods; influence of RdCVF (d term) and consumption of nutrient by cones (γ term) are considered negligible in this context. As we shall show below, the Wilk *et al.* [67] spatially-dependent photoreceptor OS length data is fit well by this reduced model.

We make a final note related to a stability property of the equilibria reported in the model of Camacho *et al.* [10]. In their model, which matches equations (1)–(3) with the parameter $\kappa^{CW} = 0$, they point out that equilibria with both $\mathcal{R}_n^{CW}$ and $\mathcal{C}^{CW}$ nonzero (i.e. coexistence of rods and cones) is not possible without a nonzero value for d_n, the RdCVF term. While we do not explore detailed stability analyses of the equilibrium solutions in our model, it does appear, based on our numerical solutions of our dynamic model, that nonzero values of $\bar{r}_{\text{eq}}$ and $\bar{c}_{\text{eq}}$ are possible in our model even in the absence of the RdCVF term ($d = 0$).

4. Comparison With Camacho & Wirkus ODE Model

Our model given by equations (9), (16), and (24) accounts for the spatial and temporal dependence of the rod and cone OS lengths and nutrient concentration. Using the appropriate integration over the retina, however, we can identify averaged variables that compare directly with those in the Camacho & Wirkus [15] model in (1)–(3).

The Camacho & Wirkus variables $\mathcal{R}_n^{\text{CW}}$ and $\mathcal{C}^{\text{CW}}$ can be viewed as

$$\mathcal{R}_n^{\text{CW}} = \sum_{i=1}^{\mathcal{N}_R^{\text{CW}}} \frac{\text{OS length of rod } i}{r_{\text{normal}}}, \quad \mathcal{C}^{\text{CW}} = \sum_{i=1}^{\mathcal{N}_C^{\text{CW}}} \frac{\text{OS length of cone } i}{c_{\text{normal}}}, \tag{42}$$

where $\mathcal{N}_R^{\text{CW}}$ is the total number of rods (including full and partial length rods) and

$\mathcal{N}_C^{\mathrm{CW}}$ is the total number of cones (including full and partial length cones). Our analog quantities where rod and cone OS lengths and densities are spatially dependent are

$$\mathcal{R}_n = \int_{\Omega_{\mathrm{retina}}} \frac{r}{r_{\mathrm{normal}}} R dA, \quad \mathcal{C} = \int_{\Omega_{\mathrm{retina}}} \frac{c}{c_{\mathrm{normal}}} C dA, \tag{43}$$

where Ω_{retina} is the two-dimensional region associated with the retina. We can also define analog total numbers of rods and cones for our model by

$$\mathcal{N}_R = \int_{\Omega_{\mathrm{retina}}} R dA, \quad \mathcal{N}_C = \int_{\Omega_{\mathrm{retina}}} C dA. \tag{44}$$

The Camacho & Wirkus model works with the number of full length rods (or cones) so that, for example, $\mathcal{R}_n^{\mathrm{CW}} = \mathcal{N}_C^{CW} \times r_{\mathrm{mean}}^{CW}/r_{\mathrm{normal}}$ where r_{mean}^{CW} represents the mean rod length across the retina and the individual factors are not resolved in their model.

The Camacho & Wirkus nutrient variable is the total number of RPE cells, $\mathcal{T}^{CW}$. Our *concentration* T integrated over the region $\Omega_{\mathrm{nutrient}}$ where the nutrient is located represents the total amount of available nutrient at a given time. If η is a conversion factor for the amount of available nutrient per RPE cell (units: mol RPE^{-1}) then

$$\eta \mathcal{T} \;=\; \int_{\Omega_{\mathrm{nutrient}}} T dV, \tag{45}$$

where $\mathcal{T}$ is a quantity that represents the total number of RPE cells analogous to $\mathcal{T}^{\mathrm{CW}}$.

A direct comparison between the Camacho & Wirkus [15] formulation and ours follows by rewriting their variables in terms of rod and cone OS lengths and nutrient concentration under the assumption of uniformity of these quantities across the entire retina. Specifically, we make the substitutions

$$\mathcal{R}_n^{\mathrm{CW}} \to \frac{r}{r_{\mathrm{normal}}} \mathcal{N}_R^{\mathrm{CW}}, \quad \mathcal{C}^{\mathrm{CW}} \to \frac{c}{c_{\mathrm{normal}}} \mathcal{N}_C^{\mathrm{CW}}, \quad \mathcal{T}^{\mathrm{CW}} \to \frac{V_{\mathrm{nutrient}}}{\eta} T, \tag{46}$$

where V_{nutrient} is the volume occupied by the nutrient (units: liters). Then, if we insert (46) into the Camacho & Wirkus equations (1)–(3) and assume that the quantities $\mathcal{N}_R^{\mathrm{CW}}/r_{\mathrm{normal}}$, $\mathcal{N}_C^{\mathrm{CW}}/c_{\mathrm{normal}}$, and $V_{\mathrm{nutrient}}/\eta$ are independent of time, we obtain

$$\frac{dr}{dt} \;=\; r\Big[\left(a_n^{\mathrm{CW}} \frac{V_{\mathrm{nutrient}}}{\eta}\right) T - \mu_n^{\mathrm{CW}}\Big], \tag{47}$$

$$\frac{dc}{dt} = c\Big[\left(a_c^{\mathrm{CW}}\frac{V_{\mathrm{nutrient}}}{\eta}\right)T + \frac{d_n^{\mathrm{CW}}}{r_{normal}}r\mathcal{N}_R^{\mathrm{CW}} - \mu_c^{\mathrm{CW}}\Big], \tag{48}$$

$$\frac{dT}{dt} = T\Big[\Gamma^{\mathrm{CW}} - \left(\kappa^{\mathrm{CW}}\frac{V_{\mathrm{nutrient}}}{\eta}\right)T - \left(\frac{\beta_n^{\mathrm{CW}}\mathcal{N}_R^{\mathrm{CW}}}{r_{\mathrm{normal}}}\right)r - \left(\frac{\gamma^{\mathrm{CW}}\mathcal{N}_C^{\mathrm{CW}}}{c_{\mathrm{normal}}}\right)c\Big]. \tag{49}$$

Comparing these with our equations (9), (16), and (24) suggests relationships between our rate coefficients and the ones in Camacho & Wirkus [15] as listed in Table 2. We have introduced a reference rod density $R_{\mathrm{ref}}^{\mathrm{CW}} = \mathcal{N}_R^{\mathrm{CW}}/A_{\mathrm{retina}}$ (units: Rod OS m^{-2}) and a reference cone density $C_{\mathrm{ref}}^{\mathrm{CW}} = \mathcal{N}_C^{\mathrm{CW}}/A_{\mathrm{retina}}$ (units: Cone OS m^{-2}). We have also introduced dimensionless scale factors f_r and f_c with the recognition that, in our work, we include logistic type terms involving factors $\ell_r - r$ and $\ell_c - c$, which are not present in the Camacho & Wirkus formulation. That is, in order to compare Camacho & Wirkus parameters with ours we loosely associate f_r with $(\ell_r - r)/r_{\mathrm{normal}}$ and f_c with $(\ell_c - c)/c_{\mathrm{normal}}$ in the relations listed in Table 2. Expressions $(\ell_r - r)/r_{\mathrm{normal}}$ and $(\ell_c - c)/c_{\mathrm{normal}}$ are space and time dependent and so the interpretation of f_r and f_c would be as appropriate scales for these quantities. In our calculations presented below comparing to the Guérin *et al.* [28, 29] data we use for simplicity $f_r = f_c = 1$. We further note that since the quantities ℓ_r and ℓ_c have no analogs in the Camacho & Wirkus model we make not attempt in this context to identify their appropriate values. Numerical values for ℓ_r and ℓ_c will be identified below when we compare our model predictions to data from Guérin *et al.* [28, 29] and to data from Wilk *et al.* [67].

Although we have just demonstrated the connections between our model and that of Camacho & Wirkus [15] we reiterate the key differences and extensions here:

- Our model distinguishes between photoreceptor OS length and photoreceptor density (for each type of photoreceptor: rods and cones) instead of treating the photoreceptor lengths as cumulative variables across the entire retina.

- Existing measurements of rod and cone density dependence on position across the retina are incorporated into our model, which effectively gives spatially-dependent

Parameter	Relation to Camacho & Wirkus [15]	Units
a_r^*	$a_r^* = a_n^{\mathrm{CW}} V_{\mathrm{nutrient}}/(\eta r_{\mathrm{normal}} f_r)$	$\mathrm{M}^{-1}\ \mathrm{m}^{-1}\ \mathrm{s}^{-1}$
μ_r^*	$\mu_r^* = \mu_n^{\mathrm{CW}}$	s^{-1}
a_c^*	$a_c^* = a_c^{\mathrm{CW}} V_{\mathrm{nutrient}}/(\eta c_{\mathrm{normal}} f_c)$	$\mathrm{M}^{-1}\ \mathrm{m}^{-1}\ \mathrm{s}^{-1}$
μ_c^*	$\mu_c^* = \mu_c^{\mathrm{CW}}$	s^{-1}
d^*	$d^* = d_n^{\mathrm{CW}} A_{\mathrm{retina}}/(r_{\mathrm{normal}} c_{\mathrm{normal}} f_c \Delta A)$	Rod $\mathrm{OS}^{-1}\ \mathrm{m}^{-2}\ \mathrm{s}^{-1}$
Γ^*	$\Gamma^* = \Gamma^{\mathrm{CW}}$	s^{-1}
κ^*	$\kappa^* = \kappa^{\mathrm{CW}} V_{\mathrm{nutrient}}/\eta$	$\mathrm{s}^{-1}\ \mathrm{M}^{-1}$
β^*	$\beta^* = \beta_n^{\mathrm{CW}} A_{\mathrm{retina}}/(r_{\mathrm{normal}}^2 f_r)$	Rod $\mathrm{OS}^{-1}\ \mathrm{s}^{-1}$
γ^*	$\gamma^* = \gamma^{\mathrm{CW}} A_{\mathrm{retina}}/(c_{\mathrm{normal}}^2 f_c)$	Cone $\mathrm{OS}^{-1}\ \mathrm{s}^{-1}$

Table 2: Dimensional parameter values in our equations (9), (16), and (24) and their relation to Camacho & Wirkus [15] parameters. Note that V_{nutrient} and η appear only the combination $V_{\mathrm{nutrient}}/\eta$. We note that the dimensionless parameters appearing in our dimensionless model do not require specification of either $V_{\mathrm{nutrient}}/\eta$ or ΔA, which appears in d^* (see Table 3).

coefficients in our dynamic model. Our working variables – rod OS length, cone OS length, and nutrient concentration – are functions of both space and time.

- Our model can be solved with or without the effects of nutrient diffusion.
- Rod and cone OS renewal is modeled with logistic terms, which set upper limits on rod and cone OS lengths at any given location across the retina. The corresponding consumption of nutrient is also limited by similar logistic terms.

If we write the Camacho & Wirkus [15] model in dimensionless form using

$$\bar{\mathcal{R}} = \frac{\mathcal{R}_n}{\mathcal{N}_R^{\mathrm{CW}}}, \quad \bar{\mathcal{C}} = \frac{\mathcal{C}}{\mathcal{N}_C^{\mathrm{CW}}}, \quad \bar{\mathcal{T}} = \frac{\mathcal{T}}{(\Gamma^{\mathrm{CW}}/\kappa^{\mathrm{CW}})}, \quad \bar{t} = \frac{t}{(1/\Gamma^{\mathrm{CW}})}, \tag{50}$$

we arrive at the dimensionless governing equations

$$\frac{d\bar{\mathcal{R}}}{d\bar{t}} = \bar{\mathcal{R}}\Big(a_r \bar{\mathcal{T}} - \mu_r\Big), \tag{51}$$

Dimensionless Parameter	Relation to Camacho & Wirkus [15]	Value
$f_r a_r$	$f_r a_r = a_n^{\mathrm{CW}}/\kappa^{\mathrm{CW}}$	0.086 to 0.092
μ_r	$\mu_r = \mu_n^{\mathrm{CW}}/\Gamma^{\mathrm{CW}}$	0.064 to 0.074
$f_c a_c$	$f_c a_c = a_c^{\mathrm{CW}}/\kappa^{\mathrm{CW}}$	0.090 to 0.096
μ_c	$\mu_c = \mu_c^{\mathrm{CW}}/\Gamma^{\mathrm{CW}}$	0.067 to 0.078
$f_c d$	$f_c d/(A_{\mathrm{retina}} R_{\max}) = d_n^{CW}/\Gamma^{\mathrm{CW}}$	0.58×10^{-11} to 0.99×10^{-11}
$f_r \beta$	$f_r \beta/(A_{\mathrm{retina}} R_{\max}) = \beta_n^{CW}/\Gamma^{\mathrm{CW}}$	0.64×10^{-9} to 0.70×10^{-9}
$f_c \gamma$	$f_c \gamma/(A_{\mathrm{retina}} C_{\max}) = \gamma^{\mathrm{CW}}/\Gamma^{\mathrm{CW}}$	2.92×10^{-8} to 3.83×10^{-8}
D	$D = D^*/(\Gamma^{\mathrm{CW}} R_{\mathrm{retina}}^2)$	$\mathcal{O}(10^{-2})$

Table 3: Dimensionless parameter in equations (32)–(34) and their relation to Camacho & Wirkus [15] parameters (see their Table 1). For D^* we use the value $1.73 \times 10^{-11}\mathrm{m}^2\ \mathrm{s}^{-1}$ quoted in Roberts [51] as an estimate. In our calculations we shall consider a range of values for D from zero up to the value listed here. The dimensionless scale factors f_r and f_c can be introduced to account presence of the logistic terms in our model as different from those in Camacho & Wirkus.

$$\frac{d\bar{\mathcal{C}}}{d\bar{t}} = \bar{\mathcal{C}}\Big(a_c\bar{\mathcal{T}} - \mu_c + d\bar{\mathcal{R}}\Big), \tag{52}$$

$$\frac{d\bar{\mathcal{T}}}{dt} = \bar{\mathcal{T}}\Big(1 - \bar{\mathcal{T}} - \beta\bar{\mathcal{R}} - \gamma\bar{\mathcal{C}}\Big). \tag{53}$$

With the exception of the diffusion coefficient, the coefficients appearing in (51)–(53) match those appearing in our dimensionless model in (32)–(34).

5. Comparison With Guérin *et al.* Retinal Reattachment Data

Guérin *et al.* [28, 29] reported experimental measurements of time-dependent growth of rod and cone OS in Rhesus Monkeys after retinal detachment/reattachment. In their studies, the retinal detachment occurred in the macula, which is the region in the functional center of the eye surrounding the fovea. Guérin *et al.* [28] indicated that in most of the cases the entire macula was detached and in no case was less than

50% of the macula detached. The retina was detached from the RPE for seven days and significant loss of rod and cone OS length in the macular region was observed over that time period, while the rod and cone inner segments remained intact. After seven days the retina was reattached and measurement of rod and cone OS length regrowth was observed for up to 150 days. The Guérin *et al.* [29] data on this photoreceptor regrowth, along with their control data, is reproduced here in Table 4.

	OS Length				
Photoreceptor	7 day (μm)	14 day (μm)	30 day (μm)	150 day (μm)	Control (μm)
Rod (mean)	8.7	9.9	13.0	32.2	29.2
(sd)	2.4*	2.3*	4.3	2.3	3.2
(min)	2	6	2	26	20
(max)	16	16	24	36	36
Cone (mean)	6.5	7.2	9.6	15.8	19.7
(sd)	2.2*	2.7*	2.9	2.9	2.3
(min)	2	2	1	8	12
(max)	14	14	20	22	28

Table 4: Photoreceptor OS recovery data from Guérin *et al.* [29], showing the mean length, standard deviation (sd), minimum length (min), and maximum length (max) measured over the macular region of the retina. Note: the standard deviation values for 7 and 14 days appear to have typographical errors in the Guérin *et al.* Figure 1 as 0.24, 0.23 (for rods) and 0.22, 0.27 (for cones), which we have corrected in our table.

Guérin *et al.* [28, 29] do not specifically report size information (diameter or area) for the macular regions in their study. However, other studies using Rhesus Monkeys [70] and humans [46, 69] have, for example, performed OCT scans to measure features of the macular region along circles of diameter ranging from 1 mm up to 6 mm centered at the fovea. Based on this, for our purposes we shall approximate the macular region as

a circular region of diameter 5 mm around the fovea, which in our model corresponds to angle θ in the range $[\theta_{\text{fovea}}, \theta_{2.5\text{mm}}]$. Here we interpret $\theta_{2.5\text{mm}} = 2.5/R_{\text{retina}}$ where $R_{r\text{etina}}$ is given in units of mm. The initial conditions used to start simulations with our model will be a 'patch' of low rod and cone OS lengths in this region of the retina, with normal values of the initial nutrient T. Outside of this patch the rod and cone OS lengths and nutrient level will be assumed to be in a normal range. In particular, in our computations shown below, we solve equations (32)–(34) on $\theta \in [\theta_{\text{fovea}}, \theta_{\text{oraserrata}}]$ subject to the initial conditions that $\bar{T}(\theta, \bar{t} = 0) = 1$ along with

$$\bar{r}(\theta, \bar{t} = 0) = \begin{cases} \bar{r}^{\text{amp}}_{\text{detached}} & \theta_{\text{fovea}} \leq \theta \leq \theta_{2.5\text{mm}} \\ \bar{r}_{\text{eq}} & \theta_{2.5\text{mm}} < \theta \leq \theta_{\text{oraserrata}} \end{cases}, \tag{54}$$

$$\bar{c}(\theta, \bar{t} = 0) = \begin{cases} \bar{c}^{\text{amp}}_{\text{detached}} & \theta_{\text{fovea}} \leq \theta \leq \theta_{2.5\text{mm}} \\ \bar{c}_{\text{eq}} & \theta_{2.5\text{mm}} < \theta \leq \theta_{\text{oraserrata}} \end{cases}, \tag{55}$$

where $\bar{r}^{\text{amp}}_{\text{detached}}$ and $\bar{c}^{\text{amp}}_{\text{detached}}$ are dimensionless initial rod and cone OS lengths in the detached region whose values will be chosen as part of a parameter estimation procedure outlined below. The quantities $\bar{r}_{\text{eq}}$ and $\bar{c}_{\text{eq}}$ are equilibrium rod and cone OS lengths from equations (36) and (41) assuming $\bar{T}_{\text{eq}} = 1$.

We will use the rod and cone density functions for Rhesus Monkeys from Adams *et al.* [2] as shown in Table 1. Additionally, we take $r_{\text{normal}} = 29.2$ μm and $c_{\text{normal}} = 19.7$ μm, which correspond to the 'control' group reported by Guérin *et al.* [29]. In the sections below we show results of an optimization procedure that we use to select parameter values in our model, accounting for the connections to the Camacho & Wirkus [15] ODE model parameter estimates. In particular, we aim to minimize the function

$$J_G = \sum_{i=1}^{4} \left[(r^i_{\text{mean}} - r_{\text{mean}}(t_i))^2 + (c^i_{\text{mean}} - c_{\text{mean}}(t_i))^2 \right], \tag{56}$$

where r^i_{mean} and c^i_{mean} for $i = 1, 2, 3, 4$ are the four measurements of mean rod OS length and cone OS length at times t_i (7, 14, 30, 150 days) from Guérin *et al.* listed

in Table 4 and $r_{\text{mean}}(t_i)$ and $c_{\text{mean}}(t_i)$ are our numerically-computed mean rod and cone OS lengths over the region $[\theta_{\text{fovea}}, \theta_{2.5\text{mm}}]$. We show predictions for cases with and without nutrient diffusion. The optimization problem was solved numerically using `Matlab`'s `fmincon` with the `interior-point` method used for the search (although we have also tested `sqp` and found similar results).[1]

5.1. Zero Diffusion

For the zero diffusion case we use values of a_r, μ_r, a_c, μ_c, d, β, and γ based on the Camacho & Wirkus [15] paper consistent with those listed in Table 3 (with $f_r = f_c = 1$). Values for these seven quantities are shown in Table 5 as 'Fixed Parameters'. The values for C_{max}, R_{max}, and A_{retina} are as listed for the Rhesus Monkey data in Table 1.

Other parameters that appear in our model relate to the logistic terms in the rod OS and cone OS evolution equations, $\bar{\ell}_r$ and $\bar{\ell}_c$. We additionally allow $1/\Gamma^*$, the dimensional time scale, to be fit. As noted above, the dimensionless values of the rod OS and cone OS length at time zero, denoted by $\bar{r}^{\text{amp}}_{\text{detached}}$ and $\bar{c}^{\text{amp}}_{\text{detached}}$, are also fit. Optimal parameter values for $\bar{\ell}_r$, $\bar{\ell}_c$, Γ^*, $\bar{r}^{\text{amp}}_{\text{detached}}$, and $\bar{c}^{\text{amp}}_{\text{detached}}$ are shown in Table 5 for both zero and nonzero values of the diffusion coefficient, D.

Our predictions for mean rod and cone OS lengths are shown in Figure 2. Here we also plot the predicted maximum and minimum values of rod and cone OS lengths over the regrowth region and indicate the corresponding measured values from Guérin *et al.* [29]. The comparison of the mean lengths is excellent. The range given by the predicted maximum and minimum values of the rod and cone OS lengths is partially consistent with the observations as well; our computed spread increases over time and is a bit larger (smaller) compared to experiments for the rods (cones). The spatial

[1] Certain commercial products are identified here and elsewhere in this paper in order to specify the computational procedure adequately. Such identification is not intended to imply recommendation or endorsement by the National Institute of Standards and Technology, nor is it intended to imply that the materials or equipment identified are necessarily the best available for the purpose.

Fixed Parameters

a_r	μ_r	a_c	d	μ_c	β	γ
0.090	0.071	0.094	0.00029	0.075	0.022	0.58

D	Fit Parameters					J_G
	$\bar{\ell}_r^*$	$\bar{\ell}_c^*$	Γ^* (day^{-1})	$\bar{r}^{\text{amp}}_{\text{detached}}$	$\bar{c}^{\text{amp}}_{\text{detached}}$	
0	2.16	1.85	0.26	0.29	0.34	0.63
10^{-4}	2.15	1.84	0.26	0.29	0.34	0.64
10^{-3}	2.12	1.81	0.26	0.29	0.34	0.65
10^{-2}	2.07	1.77	0.27	0.29	0.34	0.68

Table 5: Fixed parameter values and fitted parameter values related to our comparisons with the photoreceptor regeneration data from Guérin *et al.* [29]. The values listed in the upper table were chosen based on the listed values in Camacho & Wirkus [15]. In the lower table, the predictions of the mean rod OS length and cone OS lengths were fit to the corresponding measurements from Guérin *et al.* over the macular region. For each listed value of the diffusion coefficient, D, the other five parameters were chosen to minimize the objective function defined in equation (56).

forms of the variation of our minimum and maximum values can be observed in space–time plots in Figure 3. Spatial variation of rod and/or cone OS lengths could be one source of variation reported in the experimental measurements but certainly a range of different regrowth rates (in time), as well as variation across different Rhesus Monkey subjects could also contribute to the experimentally-observed variations in photoreceptor OS lengths. An observation that can be made from the rod and cone OS lengths plotted versus space and time in Figure 3 is that the recovery of the photoreceptor OS length appears slowest at the centermost portion of the retina where the cone photoreceptor density is its largest. The same can be said about the rod OS lengths but this observation has less significance for rods as the rod density, in contrast to the cone

density, is minimal at the fovea.

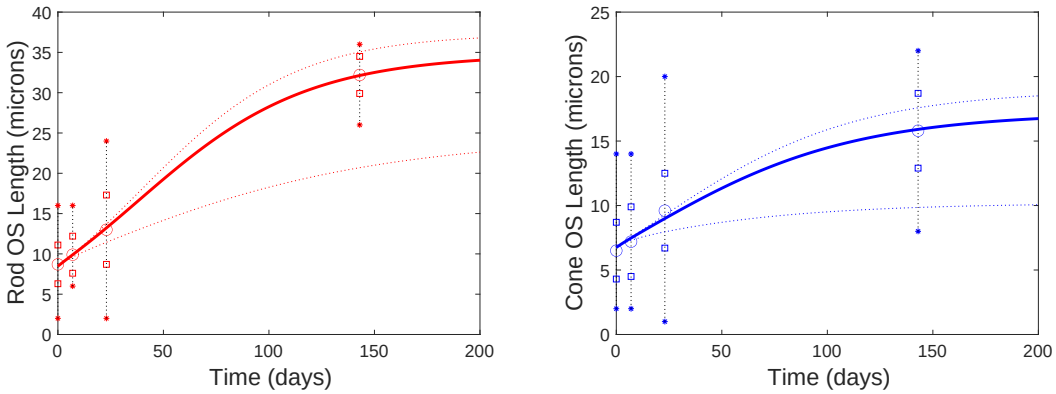

Figure 2: Rod OS and cone OS length predictions in the macula ($\theta \in [\theta_{\text{fovea}}, \theta_{2.5\text{mm}}]$) versus time. These results use the parameter values shown in Table 5 with $D = 0$. The solid lines show our computed mean OS lengths on this interval and the light dashed lines indicate the computed maximum and minimum values of the OS lengths over this same region of the retina. The data from Guérin *et al.* [29] is shown by the large circles (mean OS lengths), medium squares (mean $\pm$ standard deviation), and small stars (maximum and minimum). The corresponding dimensionless rod OS and cone OS lengths over space and time for the whole retina, including both the macula where the retina was detached and the healthy portion of the retina are shown in the next figure.

5.2. Nonzero Diffusion

The predictions for nonzero diffusion require the application of boundary conditions at $\theta = \theta_{\text{fovea}}$ and $\theta = \theta_{\text{oraserrata}}$. We use $\partial T/\partial\theta = 0$ at both boundaries and note a particular detail for implementing this condition numerically at $\theta = 0$ in the Appendix. Solutions are computed numerically using a method of lines approach and a finite difference approximation of the spatial derivative terms with the domain in $\theta \in [\theta_{\text{fovea}}, \theta_{\text{oraserrata}}]$ divided into N_θ equal intervals. We have used $N_\theta = 200$ primarily but have also observed that results with $N_\theta = 400$, 800, and 1600 show almost imperceptible differences in these graphical predictions.

Example results with nonzero diffusion coefficient are shown in Figures 4 and 5 (for $D = 10^{-3}$). The corresponding numerical values for the fit parameters are shown in

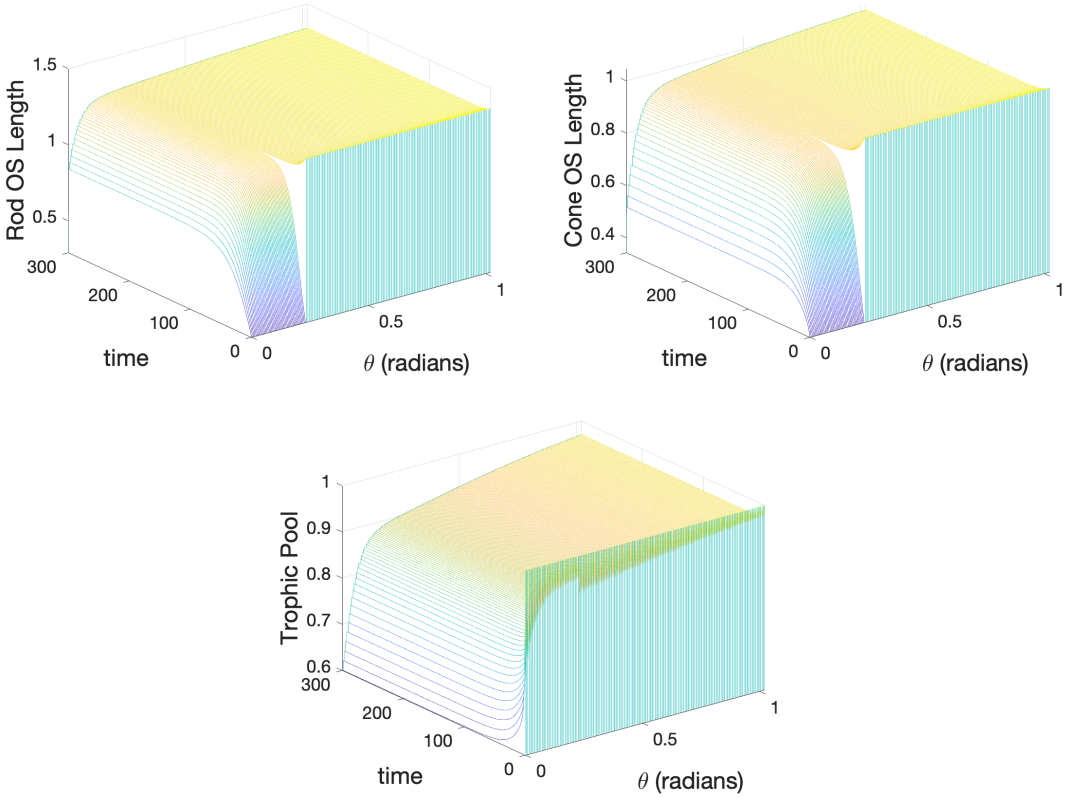

Figure 3: Dimensionless rod and cone OS lengths and nutrient concentrations for the zero-diffusion solutions shown in the previous figure comparing with the Guérin *et al.* [29] retina reattachment data.

Table 5 along with results for other values of D. We can observe that, as expected, the diffusion of nutrient reduces the spatial variation of nutrient concentration and, consequently, reduces the spatial variation of the rod OS and cone OS lengths. Specifically this can be observed in the predicted maximum and minimum OS length curves in Figure 4. From Table 5 we can also observe that the fitted parameters appear to depend weakly on the diffusion coefficient in this setting.

Note that in this particular case the parameters that also appear in Camacho & Wirkus [15] are, with one exception, taken to have the same value here as there. The exception to this is the value of Γ^* here ranges from 0.26 day^{-1} to 0.27 day^{-1} which differs from the value of $\Gamma^{\mathrm{CW}} \approx 1.5$ day^{-1} estimated by Camacho & Wirkus [15] (see

their Table 1). Also, note that a typical dimensionless value for $\bar{\ell}_r$ is slightly larger than 2 indicating that the dimensional ℓ_r is a little more than twice the normal rod OS length r_{normal}. Similarly, ℓ_c is slightly less than twice the normal cone OS length c_{normal}.

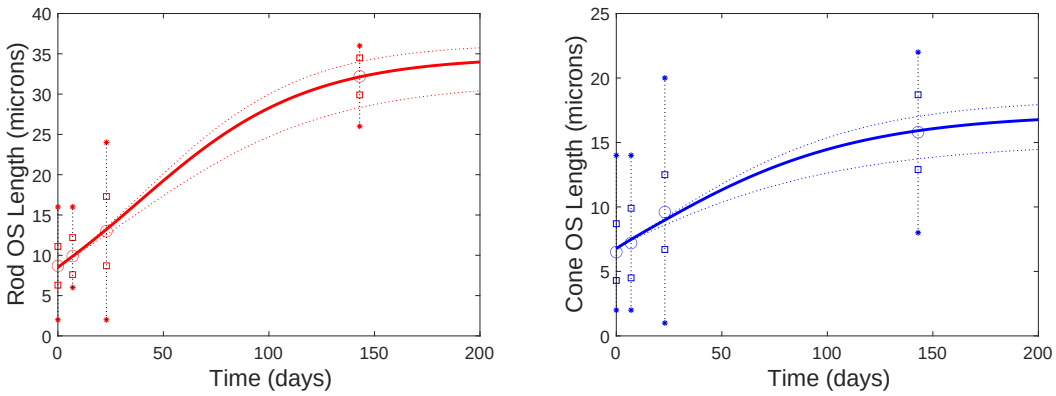

Figure 4: Rod OS and Cone OS length predictions in the macula ($\theta \in [0, \theta_{2.5\text{mm}}]$) versus time. These results use the parameter values shown in Table 5 with $D = 10^{-3}$. The line and symbol formats match the description listed in Figure 2.

6. Comparison With Wilk *et al.* Spatially-Dependent OS Length Data

Wilk *et al.* [67] reported various measurements of OS lengths in the region near the fovea for the human retina. For example, their Table 1 shows maximum and minimum values of OS lengths over a 500 μm range near the fovea as well as measurements at the 2 mm distance. Additionally, several of their OCT images show variation of the OS lengths over a range that extends out to approximately 2.5 mm from the fovea. Wilk *et al.* reported measurements for both normal subjects as well as for subjects with albinism. In keeping with our focus on the healthy eye, we use only their data for normal subjects. We assume that these data correspond to equilibrium, or steady state, configurations of the retinal photoreceptors.

More specifically, in addition to the three columns of data for normal subjects in Table 1 of Wilk *et al.* [67], we also have extracted approximate OS length data from

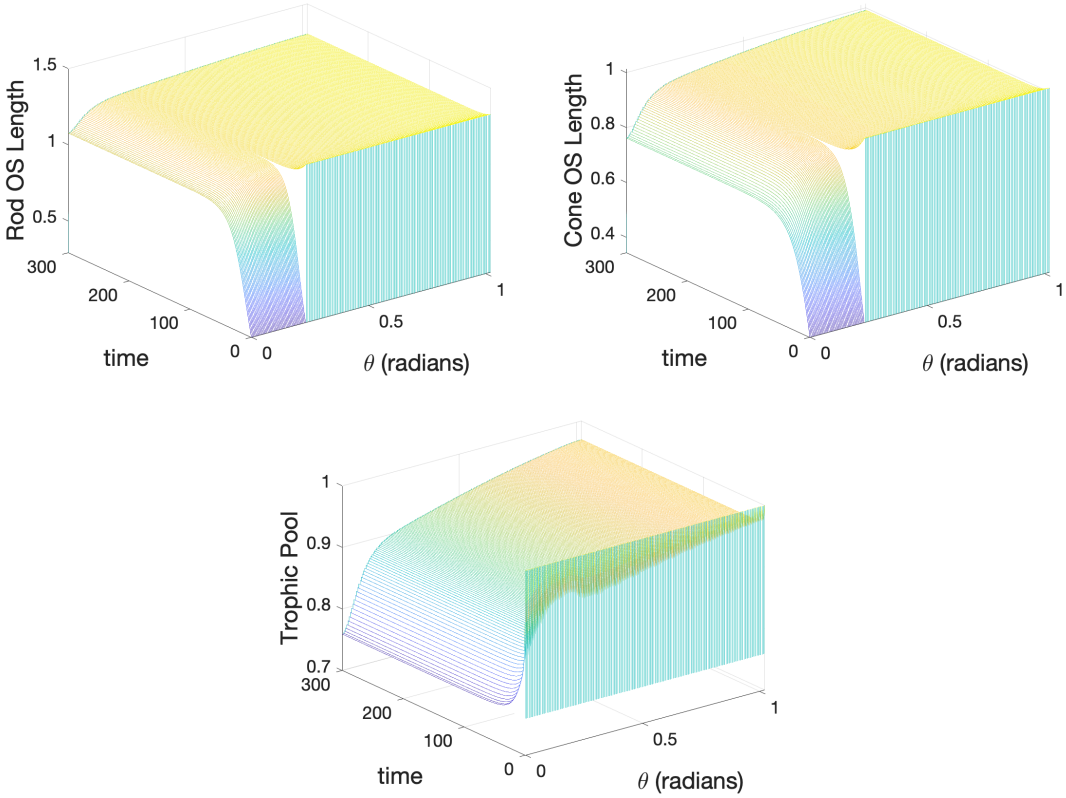

Figure 5: Dimensionless rod and cone OS lengths and nutrient concentrations for the solutions shown in the previous figure comparing with the Guérin *et al.* [29] retina reattachment data.

images in their Figures 1 and 2. These were obtained by loading the images into `Matlab` and using the `grabit.m` software to approximate the OS length at different distances from the fovea (see our Appendix, Tables B.8 and B.9). While this data acquisition methodology is not as accurate as their very careful measurements, it does provide us considerably more lower resolution data that we can use to help inform our model. The data we collected in this way gave us a set of OS length data from their Figure 1 of the form

$$\vec{P}_i^{(1)} = (\theta_i^{(1)}, OSL_i^{(1)}), \tag{57}$$

for $i = 1, \ldots, N_1$ where $N_1 = 19$ (see our Table B.8). From their Figure 2 we extracted

similar results for their two chosen subjects in the left and right plots and obtained two sets of points of the form

$$\vec{P}_i^{(2\ell)} = (\theta_i^{(2\ell)}, OSL_i^{(2\ell)}), \quad \vec{P}_i^{(2r)} = (\theta_i^{(2r)}, OSL_i^{(2r)}), \tag{58}$$

for $i = 1, \ldots, N_{2\ell}$ and $i = 1, \ldots, N_{2r}$, respectively, where $N_{2\ell} = 24$ and $N_{2r} = 25$ (see our Table B.9).

We then defined the following optimization problem. Minimize

$$J_W = J_C + J_R, \tag{59}$$

where J_C and J_R are evaluated at some sufficiently large time t_F (in the dynamic model) or using our equilibrium solutions as

$$J_C = \sum_{i=1}^{N_1} \bar{C}(\theta_i^{(1)}) * (c(\theta_i^{(1)}, t = t_F) - OSL_i^{(1)})^2, \tag{60}$$

$$J_R = \sum_{i=1}^{N_1} \bar{R}(\theta_i^{(1)}) * (r(\theta_i^{(1)}, t = t_F) - OSL_i^{(1)})^2, \tag{61}$$

subject to the constraints that

$$OSL_0^{\min} \leq c(0, t = t_F), r(0, t = t_F) \leq OSL_0^{\max}, \tag{62}$$

$$OSL_0^{\min} \leq c(\theta_{0.5\text{mm}}, t = t_F), r(\theta_{0.5\text{mm}}, t = t_F) \leq OSL_0^{\max}, \tag{63}$$

$$OSL_{2\text{mm}}^{\min} \leq c(\theta_{2.0\text{mm}}, t = t_F), r(\theta_{2.0\text{mm}}, t = t_F) \leq OSL_{2\text{mm}}^{\max}, \tag{64}$$

where $OSL_0^{\min}$ is the minimum of the 'minimum' OS length values reported for normal subjects, $OSL_0^{\max}$ is the maximum of the 'maximum' OS length values reported for normal subjects, and $OSL_{2\text{mm}}^{\min}$ and $OSL_{2\text{mm}}^{\max}$ are the minimum and maximum values of the normal subject OS length values reported for normal subjects for 2 mm (see Wilk *et al.* Table 1). Our computational procedure to find r and c does not necessarily return values at the indicated values such as $\theta_i^{(1)}$ but we compute the solution estimates at such points by linear interpolation between the neighboring points on the computational grid

for θ. In the objective function J_W we have introduced weighting factors based on the rod and cone densities, $\bar{R}(\theta)$ and $\bar{C}(\theta)$, that depend on the location θ. For example, at the fovea ($\theta = 0$) the weight for the rod contribution is zero. Similarly, the weight on the cone OS lengths as θ moves away from the fovea region decreases in proportion to the cone density. We do require that in the nonlinear inequality constraints (62)–(64) all rod and cone lengths still fall within the expected photoreceptor OS length 'goalposts'. In this particular context, the Wilk *et al.* data represents photoreceptor OS lengths and so our rod OS and cone OS predictions are fit to the same data (i.e. rod OS and cone OS lengths are effectively equivalent).

The Wilk *et al.* photoreceptor OS length data are shown in Figure 6 as small red circles (our goalposts), red crosses (actual OS length data used in the fitting), and large blue circles (not used for fitting and just shown for visual reference). We see that the photoreceptor OS lengths decrease monotonically at least out to approximately 2.5 mm from the fovea ($\theta \approx 0.25$ radians). In the context of our equilibrium model this suggests that $d\bar{r}_{\text{eq}}/d\theta < 0$ and $d\bar{c}_{\text{eq}}/d\theta < 0$ over this region. Several of our numerical comparisons to these data are also shown and these solutions are described in more detail later in this section.

Solutions of our full dynamic model require specification of the ten parameters

$$a_r, \quad \mu_r, \quad a_c, \quad d, \quad \mu_c, \quad \beta, \quad \gamma, \quad D, \quad \bar{\ell}_r, \quad \bar{\ell}_c. \tag{65}$$

Comparison with dimensional OS length data requires specification of c_{normal} and r_{normal}. We assume that $c_{\text{normal}} = r_{\text{normal}} = 55\ \mu$m, which are representative of typical photoreceptor lengths near the fovea as reported in Wilk *et al.* [67]. Since our comparison to experimental data will be made under equilibrium conditions as noted in the section on equilibria a reduced set of parameters is relevant. With the additional assumption that $\bar{\ell}_r = \bar{\ell}_c = \bar{\ell}$ and that D will be specified as a fixed parameter rather than treated as an adjustable (fitted) parameter this leads us to the reduced set of six

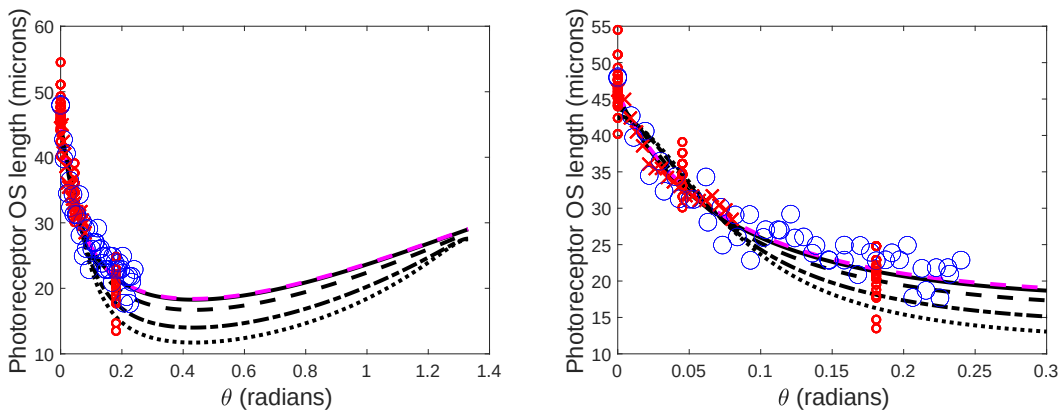

Figure 6: Dimensional photoreceptor OS length (left plot) and a zoomed-in version (right plot) as a function of angle measured from the fovea for several different values of the diffusion coefficient. Various data from Wilk *et al.* are also shown. The small red circles at $\theta = 0$ are the 'maximum' OS lengths reported in Wilk *et al.* Table 1. The small red circles at $\theta = \theta_{0.5\text{mm}}$ are the 'minimum' OS lengths reported in Wilk *et al.* Table 1. The small red circles at $\theta = \theta_{2.0\text{mm}}$ are the 2 mm OS lengths reported in Wilk *et al.* Table 1. The red crosses are the points $\vec{P}_i^{(1)}$ used in the objective function. The large blue circles are collectively the points $\vec{P}_i^{(2\ell)}$ (normal Wilk *et al.* subject with low peak density) and $\vec{P}_i^{(2r)}$ (normal Wilk *et al.* subject with highest peak density) shown for reference but otherwise not used in the optimization problem. Several cases from the results in Table 6 with $\mathcal{P}_3 \neq 0$ are shown (solid curves: $D = 0$), (dashed curves: $D = 10^{-4}$), (dash-dotted curves: $D = 10^{-3}$), and (dotted curves: $D = 10^{-2}$). The dashed magenta curve is the analytical approximation given by equation (75). The corresponding nutrient concentration is shown in Figure 7.

parameters

$$p_r = \frac{\mu_r}{a_r}, \quad p_c = \frac{\mu_c}{a_c}, \quad p_d = \frac{d}{a_c}, \quad \beta, \quad \gamma, \quad \bar{\ell}, \tag{66}$$

to be used in the optimization problem. Our solutions reported below are those obtained by solving the equilibrium problem numerically but we have also verified that the equilibrium solution reached using our dynamic model is in agreement with these equilibrium solutions.

As a first step to explore the predictions of our model in the context of the Wilk *et al.* [67] data, we solved numerically – again using `Matlab`'s `fmincon` with either the `interior-point` method or `sqp` – the optimization problem to minimize the objective

function J_W subject to the nonlinear constraints in (62)–(64) over the parameters defined in equations (66). We used a range of values $N_\theta \in [200, 1600]$. For cases with $D = 0$ a value of $N_\theta = 200$ was sufficient but when $D \neq 0$ typically we used $N_\theta = 800$ although these results were consistent with runs with $N_\theta = 400$ and 1600. The outcomes of these numerical calculations with $D \in [0, 10^{-2}]$ revealed several important results with respect to parameter estimation of our model with respect to the Wilk *et al.* data:

- The values of parameters p_d and γ appear to be near zero numerically ($p_d \approx \mathcal{O}(10^{-7})$ to $\mathcal{O}(10^{-8})$ and $\gamma \approx \mathcal{O}(10^{-8})$ to $\mathcal{O}(10^{-10})$ were typically observed). We have verified that setting $p_d = 0$ and $\gamma = 0$ provided the same numerical outcomes to within reasonable tolerances.
  - A consequence of $\gamma = 0$ is that the cone OS length variable $\bar{c}_{\text{eq}}$ decouples from equation (38) that determines the nutrient concentration.
  - A consequence of $p_d = 0$, along with the assumption that $\bar{\ell}_c = \bar{\ell}_r$ and that we fit both rod and cone OS lengths to the same photoreceptor data, is that the values of p_r and p_c appear to be effectively the same. Therefore, we define $p \equiv p_r = p_c$.
- The value of $\bar{\ell}$ remains close to, but larger than, p. This suggests a relationship $\bar{\ell} = p(1 + \varepsilon)$ where $0 < \varepsilon \ll 1$. We explore this further below.
- Predictions for $\bar{r}_{\text{eq}}$ and $\bar{c}_{\text{eq}}$ match well with the Wilk *et al.* data for the values of θ available. The nutrient concentration satisfies $0 < 1 - \bar{T}_{\text{eq}}(\theta) \ll 1$. Further details and plots are outlined below.
- Even with the reduced set of parameters assuming $p_d = 0$, $\gamma = 0$, $\bar{\ell}_r = \bar{\ell}_c = \bar{\ell}$ and $p_r = p_c = p$, individual values of p, β, and $\bar{\ell}$ are not uniquely determined by this minimization algorithm and in general depend on the initial guess as well

as the minimization scheme (e.g. `interior point` vs. `sqp`). This suggests the minimization solution we seek resides on a solution manifold within the parameter search space. We give analytical arguments and show numerical evidence that the minimization procedure determines a one-parameter family of solutions characterized by fixed values of the two parameter groups $\mathcal{P}_1 \equiv \bar{\ell} - p$, $\mathcal{P}_2 = \beta p^2$, with a third parameter group $\mathcal{P}_3 = \gamma/\beta$ apparently near zero.

We now investigate our equilibrium model in more detail. In the Wilk *et al.* context we fit $\bar{r}_{\rm eq}$ and $\bar{c}_{\rm eq}$ to the same data so it makes sense, in light of the observations just noted, to assume that $p_d = 0$ and that $\bar{\ell}_r = \bar{\ell}_c = \bar{\ell}$ and $p_r = p_c = p$. We retain $\gamma \neq 0$ for now and find that the nutrient concentration $\bar{T}_{\rm eq}$ and rod OS length $\bar{r}_{\rm eq}$ (and cone OS length $\bar{c}_{\rm eq}$) satisfy

$$0 = \bar{T}_{\rm eq}(1-\bar{T}_{\rm eq}) - \beta p \bar{r}_{\rm eq}\bar{R} - \gamma p \bar{c}_{\rm eq}\bar{C} + \frac{D}{\sin\theta}\frac{\partial}{\partial\theta}\left(\sin\theta\frac{\partial \bar{T}_{\rm eq}}{\partial\theta}\right), \tag{67}$$

$$\bar{r}_{\rm eq} = \bar{c}_{\rm eq} = \bar{\ell} - \frac{p}{\bar{T}_{\rm eq}}. \tag{68}$$

If we write $\bar{\ell} = p(1+\varepsilon)$ and also introduce $\bar{T}_{\rm eq}^{-1} = 1 + \varepsilon\bar{u}_{\rm eq}$ we find that equations (67) and (68) become

$$\begin{aligned} 0 &= \frac{\bar{u}_{\rm eq}}{(1+\varepsilon\bar{u}_{\rm eq})^2} - \beta p^2(1-\bar{u}_{\rm eq})\left(\bar{R}(\theta) + (\gamma/\beta)\bar{C}(\theta)\right) \\ &\quad - \frac{D}{\sin\theta}\frac{d}{d\theta}\left[\frac{\sin\theta}{(1+\varepsilon\bar{u}_{\rm eq})^2}\frac{d\bar{u}_{\rm eq}}{d\theta}\right], \end{aligned} \tag{69}$$

$$\bar{r}_{\rm eq} = \bar{c}_{\rm eq} = \varepsilon p\left(1-\bar{u}_{\rm eq}\right). \tag{70}$$

When $\varepsilon \ll 1$ and $\bar{u}_{\rm eq} = \mathcal{O}(1)$ as $\varepsilon \to 0$ the leading-order contributions of (69) and (70) give the approximations

$$0 \approx \bar{u}_{\rm eq} - \mathcal{P}_2(1-\bar{u}_{\rm eq})\left(\bar{R}(\theta) + \mathcal{P}_3\bar{C}(\theta)\right) - \frac{D}{\sin\theta}\frac{d}{d\theta}\left[\sin\theta\frac{d\bar{u}_{\rm eq}}{d\theta}\right], \tag{71}$$

$$\bar{r}_{\rm eq} = \bar{c}_{\rm eq} \approx \mathcal{P}_1\left(1-\bar{u}_{\rm eq}\right), \tag{72}$$

where we have introduced the three parameter groups as

$$\mathcal{P}_1 = \varepsilon p = \bar{\ell} - p, \quad \mathcal{P}_2 = \beta p^2, \quad \mathcal{P}_3 = \frac{\gamma}{\beta}, \tag{73}$$

involving the four parameters $\bar{\ell}$, p, β, and γ. Since the Wilk *et al.* [67] data give photoreceptor OS lengths versus position in the retina, we can expect our optimization procedure to inform us about the values for $\mathcal{P}_1$, $\mathcal{P}_2$, and $\mathcal{P}_3$. That is, for each specified value of D we anticipate finding a one-parameter family of solutions to our minimization problem. Below we report more details specific to cases with either $D = 0$ or $D \neq 0$.

6.1. Zero Diffusion

As written, the equilibrium problem with $D = 0$ amounts to a system of algebraic equations (36), (37), and (38) for $\bar{r}_{\text{eq}}$, $\bar{c}_{\text{eq}}$, and $\bar{T}_{\text{eq}}$ that can be solved at as few or as many values of θ as desired. While in general one must prescribe values for the six parameters in (66), as noted above, in the context of fitting to the Wilk *et al.* data it appears that one can identify solutions characterized by three parameter groups $\mathcal{P}_1$, $\mathcal{P}_2$, and $\mathcal{P}_3$. In fact, with $D = 0$ and $\varepsilon \ll 1$, a closed form expression approximating rod and cone OS lengths is possible. An approximate solution for $\bar{u}_{\text{eq}}$ in (69) is

$$\bar{u}_{\text{eq}} = \frac{\mathcal{P}_2\left(\bar{R}(\theta) + \mathcal{P}_3\bar{C}(\theta)\right)}{1 + \mathcal{P}_2\left(\bar{R}(\theta) + \mathcal{P}_3\bar{C}(\theta)\right)} + \mathcal{O}(\varepsilon), \tag{74}$$

in which case an approximation for $\bar{r}_{\text{eq}} = \bar{c}_{\text{eq}}$ is

$$\bar{r}_{\text{eq}} = \bar{c}_{\text{eq}} = \frac{\mathcal{P}_1}{1 + \mathcal{P}_2\left(\bar{R}(\theta) + \mathcal{P}_3\bar{C}(\theta)\right)} + \mathcal{O}(\varepsilon^2). \tag{75}$$

Note that from equation (75) we find that

$$\frac{d\bar{r}_{\text{eq}}}{d\theta} = \frac{d\bar{c}_{\text{eq}}}{d\theta} = -\frac{\mathcal{P}_1\left(\frac{d\bar{R}}{d\theta} + \mathcal{P}_3\frac{d\bar{C}}{d\theta}\right)}{\left[1 + \mathcal{P}_2\left(\bar{R}(\theta) + \mathcal{P}_3\bar{C}(\theta)\right)\right]^2} + \mathcal{O}(\varepsilon^2). \tag{76}$$

Also note that $d\bar{r}_{\text{eq}}/d\theta$ and $d\bar{c}_{\text{eq}}/d\theta$ appear to be negative over the values of θ for which we have Wilk *et al.* OS length data. Recall from equations (28) and (29) and also Figure 1 that $d\bar{R}/d\theta > 0$ and $d\bar{C}/d\theta < 0$ over this range of θ. Therefore, it appears that $d\bar{R}/d\theta + \mathcal{P}_3 d\bar{C}/d\theta > 0$ is needed to describe the Wilk *et al.* data and so $\mathcal{P}_3$ must not be too large. A very small value of $\mathcal{P}_3$ seems to be consistent with our numerical findings.

Numerical values for $\mathcal{P}_1$, $\mathcal{P}_2$, and $\mathcal{P}_3$ based on the comparison to the Wilk *et al.* [67] data are listed in Table 6. We have included cases in which we explicitly set $\mathcal{P}_3 = 0$ and cases in which we allow $\mathcal{P}_3 > 0$. For each different value of D there are slight differences between the reported solutions. These differences we believe are not significant given the uncertainty associated with the specific set of fit data used and more generally in light of the broad variation from one subject to the next in photoreceptor OS lengths.

Solutions for the rod and cone OS lengths $\bar{r}_{eq}$ and $\bar{c}_{eq}$ as functions of θ are shown in Figure 6 for the case where $\mathcal{P}_3 = 0$. For the case $D = 0$ solid black lines show the numerical solution and the nearly coincident dashed magenta lines show the approximate solution given by equation (75). The right plot shows the same quantities for values of θ near the range of the Wilk *et al.* data, which corresponds to approximately 2.5 mm out from the fovea. The corresponding results for nutrient concentration $\bar{T}_{eq}$ (solid black curve and coincident dashed magenta curve) are shown in Figure 7. The clear trend in the data, which is also reflected in the model predictions is a decrease in the photoreceptor OS length moving away from the fovea. Our predictions extend further and suggest that the OS length reaches a minimum and begins to increase with increasing distance from the fovea. This behavior can be linked directly to the non-monotonic structure of the rod density function $\bar{R}(\theta)$ as evident in equation (75), recalling that $\bar{C}(\theta) \to 0$ away from the fovea. Certainly it would be interesting to compare these predictions with experimental measurements of photoreceptor OS lengths further from the fovea where the rods dominate. We remark that there is information on the spatial variation of retina thickness over the whole retina. In Kolb, Fernandez, & Nelson [32] (p. 1830, Figure 3) values for retinal thickness at the foveal floor, the foveal rim, and the ora serrata are 150 μm–200 μm, 320 μm, and 80 μm, respectively. Our predictions for OS length near 30 μm at the ora serrata in Figure 6 may be more than a retinal thickness value of 80 μm would be able to accommodate given the various other sublayers in addition to the photoreceptor OS that must also occupy space

in the retina. This observation may suggest that in our model the quantities ℓ_r and ℓ_c are likely also spatially-dependent; potentially related to the retinal thickness, which is necessarily an upper bound on the OS length.

While equation (75) also involves the cone density function $C(\theta)$ it does not appear that there is sufficient resolution in the Wilk *et al.* [67] data near $\theta = 0$ to conclusively distinguish cases with $\mathcal{P}_3 = 0$ and $\mathcal{P}_3 \neq 0$ but small. With sufficiently large values of $\mathcal{P}_3$ our predictions for rod and cone OS lengths near $\theta = 0$ would have OS lengths increasing locally, which does not appear to be a feature of the Wilk *et al.* data. Values for $\mathcal{P}_1$ and $\mathcal{P}_2$, while certainly variable with respect to D appear to be more robustly identified by our minimization problem, but again would certainly be sensitive to the details of the OS length data (e.g. using data from a different subject).

	Best Fit Parameter Groups			
D	$\mathcal{P}_1$	$\mathcal{P}_2$	$\mathcal{P}_3$	J_W
0	0.83	1.50	0	10.00
0	0.83	1.50	2.4×10^{-6}	10.00
10^{-4}	0.93	2.02	0	29.04
10^{-4}	0.93	2.02	2.52×10^{-6}	29.04
10^{-3}	1.38	4.31	0	49.03
10^{-3}	1.38	4.31	4.27×10^{-6}	49.03
10^{-2}	5.45	21.60	0	57.81
10^{-2}	5.45	21.62	2.65×10^{-5}	57.81

Table 6: Fitted parameter groups $\mathcal{P}_1$, $\mathcal{P}_2$, and $\mathcal{P}_3$ obtained from comparisons with the Wilk *et al.* [67] photoreceptor spatial-dependence data. There are two sets of runs for each value of D; the first has $\mathcal{P}_3 = 0$ and the second allows $\mathcal{P}_3$ to vary as one of the fitted parameters. These results have assumed $p_d = 0$.

6.2. Nonzero Diffusion

The predictions for nonzero diffusion require the application of boundary conditions for T at $\theta = \theta_{\text{fovea}}$ and $\theta = \theta_{\text{oraserrata}}$. We use $\partial T/\partial\theta = 0$ at both boundaries (again note a particular detail for implementing this condition numerically at $\theta = 0$ in the Appendix). Solutions are computed numerically using a method of lines approach with the domain $\theta \in [\theta_{\text{fovea}}, \theta_{\text{oraserrata}}]$ divided into N_θ equal intervals.

Numerical values for $\mathcal{P}_1$, $\mathcal{P}_2$, and $\mathcal{P}_3$ again for cases with $\mathcal{P}_3 = 0$ and $\mathcal{P}_3 > 0$ are listed in Table 6. We see that $\mathcal{P}_1$ and $\mathcal{P}_2$ are sensitive to the value of D but $\mathcal{P}_3$ tends to remain near zero in all cases. Figure 6 shows the corresponding rod and cone OS lengths for $D = 10^{-4}$ (dashed curve), 10^{-3} (dash-dotted curve), and 10^{-2} (dotted curve). In this figure we see that increasing the diffusion coefficient has the effect of amplifying the variation in the photoreceptor OS length over intermediate angles shown, although still maintaining consistency with the Wilk *et al.* data. Again, the results of our model suggest the need for additional experimental data covering the retina away from the fovea. Again we remark that in this context the consideration of spatial dependence of ℓ_r and ℓ_c may be important. The corresponding nutrient concentration predictions are shown in Figure 7. As the diffusion coefficient increases the spatial variation in the nutrient variable in general decreases but the overall nutrient level stays near a dimensionless value of unity.

7. Conclusions

In this study we have developed a dynamic mathematical model that incorporates spatial dependence of rod and cone densities across the retina and uses this information in the prediction of rod and cone OS lengths and nutrient concentration. The model includes diffusion of nutrient and is in the form of a coupled partial differential equation system. Our mathematical model, as a PDE system that accounts for spatial dependence of critical features of the retina, has a number of connections with the ODE-based

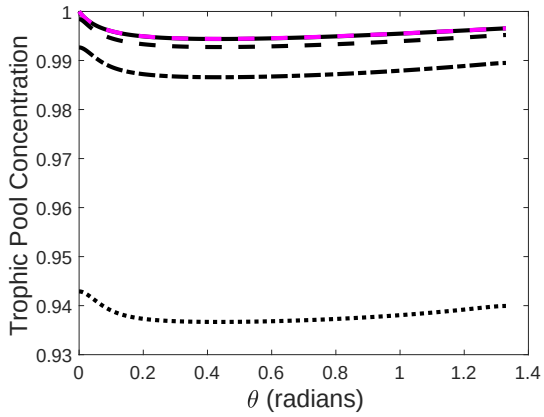

Figure 7: Dimensionless nutrient concentration $\bar{T}$ predictions as a function of angle measured from the fovea for several cases shown in Table 6 with $\mathcal{P}_3 \neq 0$ (solid curve: $D = 0$), (dashed curve: $D = 10^{-4}$), (dash-dotted curve: $D = 10^{-3}$), and (dotted curve: $D = 10^{-2}$). The dashed magenta curve is the analytical approximation $\bar{T}_{\text{eq}} = 1/(1 + \varepsilon \bar{u}_{\text{eq}})$ with $\bar{u}_{\text{eq}}$ given by equation (74). These correspond to the rod OS and cone OS predictions in Figure 6.

model of Camacho & Wirkus [15] and the PDE-based models of Roberts *et al.* [53, 51]. We have connected our model predictions to a number of different experimental measurements. First, rod and cone photoreceptor density data in the retina have been incorporated for both humans (Curcio *et al.* [21]) and Rhesus Monkeys (Adams *et al.* [2]). Second, we have used the Rhesus Monkey photoreceptor density data to make detailed comparisons with rod and cone OS dynamic regrowth data from experiments of Guérin *et al.* [28, 29]. Third, we have used the human photoreceptor density data to make comparisons with measured photoreceptor OS length data of human retinas by Wilk *et al.* [67]. Here we have derived a closed-form expression for photoreceptor OS lengths, in the absence of diffusion, that could be further tested against additional experimental data. In all cases, our ability to make comparisons to experimental data and offer testable predictions lends support to the utility of our mathematical model.[2]

[2]This meets the definition of a 'useful' model by Roberts *et al.* [52] as it 'replicates current data enabling us to make predictions'.

Given the importance of mathematical models to explore retinal diseases such as retinitis pigmentosa, we anticipate that the model presented here may be of interest for future investigations of retinal structure, function, and dynamics.

Acknowledgements

The authors would like to acknowledge one of the reviewers whose comments were particularly helpful in making several important improvements in our paper. Research funding for D.C. Brager was provided in part by the National Institute of Standards and Technology and a National Research Postdoctoral Fellowship.

Appendix A. Adams *et al.* Rhesus Monkey Photoreceptor Density Data

We record in Table A.7 the angle and photoreceptor data that we have extracted via `Matlab`'s `grabit.m` from Figure 2 in Adams *et al.* [2]. We use this as the Rhesus Monkey analog of the Curcio *et al.* [21] human photoreceptor density data. Results of the fits to this photoreceptor data are shown in Table 1.

Appendix B. Wilk *et al.* Photoreceptor OS Length Data

We have used `Matlab`'s `grabit.m` software to extract photoreceptor OS length data versus position in the retina from experimental images in Wilk *et al.* [67] Figures 1 and 2. We have identified these approximate photoreceptor OS lengths directly from their image A in Figure 1 by marking points along their upper (blue) line and lower (orange) line and extending this out to the edge of the image. We repeated a similar procedure with two images in their Figure 2. While their measurement scheme is clearly more accurate than ours, the additional quantitative information of OS length versus position appears to be accurate within the variation across subjects and is extremely helpful in our analysis. These values are listed in Table B.8. The two additional examples shown in Wilk *et al.* Figure 2 show similar detail to lower resolution but are

Angle from Fovea (Degrees)	Rod Density (mm^{-2} 10^{-3})
1.31	5.12
3.72	24.13
6.04	48.50
6.95	61.65
7.96	65.56
9.16	68.24
10.77	80.43
13.88	93.60
15.38	88.01
16.69	94.35
18.69	92.66
21.40	96.82
24.01	109.26
26.71	104.65
31.90	83.74
37.21	79.40
42.41	67.75
48.00	52.93
53.11	45.90
58.51	43.51

Angle from Fovea (Degrees)	Cone Density (mm^{-2} 10^{-3})
0.23	49.19
0.83	37.02
1.52	30.20
3.92	23.16
6.12	9.54
8.12	9.55
9.32	9.07
10.62	9.57
13.83	9.59
15.33	7.41
16.93	7.91
18.73	5.97
21.23	6.23
24.04	5.04
26.74	5.06
31.55	4.36
37.05	2.94
42.26	2.73
47.67	2.52
52.88	2.80
58.29	3.08

Table A.7: Rod and cone density data for a Rhesus Monkey collected via `Matlab`'s `grabit.m` from Adams *et al.* [2] Figure 2.

useful as they show data for two additional subjects and at points further from the fovea (e.g. out to an estimated 2500 μm to 2600 μm versus the estimated 880 μm we were able to extract from their Figure 1 and also versus their reported measurements in Table 1 at 2 mm = 2000 μm). These values are listed in Table B.9. As described in the main text, we define our objective function based on the data we extracted from Figure 1 and use the data Wilk *et al.* report in their Table 1 for normal subjects (Maximum, Minimum, and 2 mm OS lengths) as constraints in our calculations. The data we obtained from the two images in Wilk *et al.* Figure 2 are quite noisy due to

the nature of our data collection scheme and for this reason are used simply as a visual comparison of our predictions that extend further from the fovea than the data that we used in the fitting procedure. The distance from fovea data was converted to radians by interpreting these values as arclength, converting them to mm and then dividing by 11.06 mm as an estimate of the radius of a 'spherical' eye.

Distance from Fovea (μm)	Photoreceptor OS Length (μm)
0.0	46.2
52.4	45.0
97.6	42.4
145.1	40.5
192.7	38.6
240.2	36.1
290.2	35.4
339.0	35.5
384.2	34.2
430.5	33.6
479.3	33.0
528.1	31.7
579.3	31.7
630.5	31.1
680.5	31.1
731.7	31.7
782.9	30.4
836.6	29.8
885.4	28.5

Table B.8: Data collected via `Matlab`'s `grabit.m` from Wilk *et al.* Figure 1A (right side of fovea).

Distance from Fovea (μm)	Photoreceptor OS Length (μm)
0.0	47.9
104.1	42.7
212.5	40.6
329.5	36.5
446.5	34.3
559.2	31.3
682.6	34.3
797.4	30.1
908.1	29.1
1020.9	29.1
1144.3	27.1
1257.0	27.0
1369.8	25.9
1506.0	23.8
1631.6	22.9
1752.9	22.9
1876.4	24.9
1999.8	22.8
2121.2	23.9
2240.4	24.9
2353.3	21.8
2464.1	21.8
2553.6	21.8
2655.8	22.9

Distance from Fovea (μm)	Photoreceptor OS Length (μm)
0.0	48.1
122.9	39.7
243.6	34.5
358.2	32.3
474.9	31.3
589.5	31.2
697.9	28.1
810.4	24.9
925.0	26.1
1027.1	22.9
1127.2	26.0
1239.8	27.0
1337.8	29.2
1437.9	26.1
1533.8	24.9
1636.0	22.9
1752.7	24.9
1857.0	20.9
1955.0	24.0
2071.8	22.9
2180.2	22.9
2282.4	17.7
2384.5	18.7
2493.0	17.7
2568.1	21.0

Table B.9: Data collected via `Matlab`'s `grabit.m` from Wilk *et al.* Figure 2. The left table corresponds to the lower left image of Wilk *et al.* Figure 2 (right side of fovea) from a subject with low peak cone density. The right table corresponds to the lower right image of Wilk *et al.* Figure 2 (also right side of fovea) from a subject with the highest peak cone density.

Appendix C. Boundary Condition: Nonzero Diffusion

For cases in which we consider nonzero diffusion and wish to impose $\partial T/\partial\theta = 0$ at $\theta = 0$ we make the following observation. Define the diffusion terms to be

$$\mathcal{D} = \frac{1}{\sin\theta}\frac{\partial}{\partial\theta}\left(\sin\theta\frac{\partial T}{\partial\theta}\right) = \frac{\partial^2 T}{\partial\theta^2} + \frac{\cos\theta}{\sin\theta}\frac{\partial T}{\partial\theta}. \tag{C1}$$

In the limit $\theta \to 0$ it follows that

$$\begin{aligned}
\mathcal{D} &= \frac{\partial^2 T}{\partial \theta^2}(\theta = 0) + \theta \frac{\partial^3 T}{\partial \theta^3}(\theta = 0) + \mathcal{O}(\theta^2) \\
&\quad + \frac{1 + \mathcal{O}(\theta^2)}{\theta + \mathcal{O}(\theta^3)} \left(\frac{\partial T}{\partial \theta}(\theta = 0) + \theta \frac{\partial^2 T}{\partial \theta^2}(\theta = 0) + \mathcal{O}(\theta^2) \right), \\
&= 2 \frac{\partial^2 T}{\partial \theta^2}(\theta = 0) + \mathcal{O}(\theta) \qquad \text{(C2)}
\end{aligned}$$

if one imposes $\partial T/\partial\theta(\theta = 0) = 0$. So $\mathcal{D}(\theta = 0) = 2\partial^2 T/\partial\theta^2(\theta = 0)$. Consider a finite difference scheme with uniformly-spaced grid points $[\theta_1, \ldots, \theta_i, \ldots, \theta_{N_\theta+1}]$ where $\theta_i = (i-1)\theta_{\text{oraserrata}}/N_\theta$ for $i = 1, \ldots, N_\theta + 1$. If we impose $\partial T/\partial\theta = 0$ at $\theta = 0$ through the introduction of a ghost point $\theta_0 \equiv \theta_2$ (i.e. a second order accurate representation of a central difference formula for the derivative set to zero) then the application of the PDE for T at $\theta = 0$ (i.e. $i = 0$) requires that the diffusion term be written as

$$\mathcal{D}(\theta = 0) = 2 \frac{\theta_0 - 2\theta_1 + \theta_2}{\Delta\theta^2}, \qquad \text{(C3)}$$

where $\Delta\theta = \theta_{\text{oraserrata}}/N_\theta$. That is, the diffusion term picks up a factor of 2.

References

[1] T. Ach, C. Huisingh, G. McGwin Jr, J.D. Messinger, T. Zhang, M.J. Bentley, D.B. Gutierrez, Z. Ablonczy, R.T. Smith, K.R. Sloan, & C.A. Curcio. Quantitative autofluorescence and cell density maps of the human retinal pigment epithelium. *Invest. Ophth. Vis. Sci.* **55** 4832–4841 (2014) DOI: 10.1167/iovs.14-14802

[2] C.K. Adams, J.M. Perez, & M.N. Hawthorne. Rod and cone densities in the Rhesus. *Invest. Ophth.* **13** 885–888 (1974).

[3] P.K. Ahnelt. The photoreceptor mosaic. *Eye* **12** 531–540 (1998).

[4] B.L.S. Andrade da Costa & J. N. Hokoç. Photoreceptor topography of the retina in the New World monkey *Cebus apella*. *Vision Res.* **40** 2395–2409 (2000).

[5] S.K. Bhatia, A. Rashid, M.A. Chrenek, Q. Zhang, B.B. Bruce, M. Klein, J.H. Boatright, Y. Jiang, H.E. Grossniklaus, J.M. Nickerson. Analysis of RPE morphometry in human eyes. *Mol. Vis.* **22** 898–916 (2016).

[6] D. Bok. Retinal photoreceptor-pigment epithelium interactions. *Invest. Ophth. Vis. Sci.* **26** 1659–1694 (1985).

[7] A.J. Bower, T. Liu, N. Aguilera, J. Li, J. Liu, R. Lu, J.P. Giannini, L.A. Huryn, A. Dubra, Z. Liu, D.X. Hammer, & J. Tam. Integrating adaptive optics-SLO and OCT for multimodal visualization of the human retinal pigment epithelial mosaic. *Biomed. Opt. Express* **12** 1449–1466 (2021). https://doi.org/10.1364/BOE.413438

[8] J. Burns, G. Clarke, & C.J. Lumsden. Photoreceptor death: spatiotemporal patterns arising from one-hit death kinetics and a diffusible cell death factor. *B. Math. Biol.* **64** 1117–1145 (2002).

[9] A. Cakir, S.G. Ozturan, D. Yildiz, B. Erden, S. Bolukbasi, E.K. Tascilar, M.N. Yanmaz, and M.N. Elcioglu. Evaluation of photoreceptor outer segment length in hydrochloroquine users. *Eye* **33** 1321–1326 (2019) https://doi.org/10.1038/s41433-019-0425-z

[10] E.T. Camacho, M.A.C. Véez, D.J. Hernández, U.R. Bernier, J. Van Laarhoven, & S. Wirkus. A mathematical model for photoreceptor interactions. *J. Theor. Biol.* **267** 638–646 (2010) doi: 10.1016/j.jtbi.2010.09.006

[11] E.T. Camacho, S. Lenhart, L.A. Melara, M.C. Villalobos, & S. Wirkus. Optimal control with MANF treatment of photoreceptor degeneration. *Math. Med. Biol.* **37** 1–21 (2020) https://doi.org/10.1093/imammb/dqz003

[12] E.T. Camacho, T. Léveillard, J.-A. Sahel, & S. Wirkus. Mathematical model of the role of RdCVF in the coexistence of rods and cones in a healthy eye. *B. Math. Biol.* **78** 1394–1409 (2016) doi 10.1007/s11538-016-0185-x

[13] E.T. Camacho, L.A. Melara, M.C. Villalobos, & S. Wirkus. Optimal control in the treatment of retinitis pigmentosa. *B. Math. Biol.* **76** 292–313 (2014).

[14] E.T. Camacho, C. Punzo, & S.A. Wirkus. Quantifying the metabolic contribution to photoreceptor death in retinitis pigmentosa via a mathematical model. *J. Theor. Biol.* **408** 75–87 (2016) https://dx.doi.org/10.1016/j.jtbi.2016.08.001

[15] E.T. Camacho & S. Wirkus. Tracing the progression of retinitis pigmentosa via photoreceptor interactions. *J. Theor. Biol.* **317** 105–118 (2013).

[16] J.A. Cava, M.T. Allphin, R.R. Mastey, M. Gaffney, R.E. Linderman, R.F. Cooper, and J. Carroll. Assessing interocular symmetry of the foveal cone mosaic. *Invest. Ophth. Vis. Sci.* **61** 23 (2020). https://doi.org/10.1167/iovs.61.14.23

[17] T.Y.P. Chui, H. Song, & S.A. Burns. Individual variations in human cone photoreceptor packing density: variations with refractive error. *Invest. Ophth. Vis. Sci.* **49** 4679–4687 (2008).

[18] K.M. Conway. Diffusion patterns on domains representing developing *Xenopus* retina. *J. Theor. Biol.* **163** 181–197 (1993).

[19] R.F. Cooper, M.A. Wilk, S. Tarima, & J. Carroll. Evaluating descriptive metrics of the human cone mosaic. *Invest. Ophth. Vis. Sci.* **57** 2992–3001 (2016) DOI: 10.1167/iovs.16-19072

[20] R.F. Cooper, G.K. Aguirre, & J.I.W. Morgan. Fully automated estimation of spacing and density for retinal mosaics. *Trans. Vis. Sci. Tech.* **8** 26 (2019) https://doi.org/10.1167/tvst.8.5.26

[21] C.A. Curcio, K.R. Sloan, R.E. Kalina, and A.E. Hendrickson. Human photoreceptor topography. *J. Comp. Neurol.* **292** 497–523 (1990).

[22] N. Domdei, J.L. Reiniger, F.G. Holz, & W.M. Harmening. The relationship between visual sensitivity and eccentricity, cone density and outer segment length in the human foveola. *Invest. Ophth. Vis. Sci.* **62** 31 (2021) https://doi.org/10.1167/iovs.62.9.31

[23] I. Fatt & B.A. Weissman. *Physiology of the Eye: An Introduction to the Vegetative Functions.* (Butterworth–Heinemann, Boston, Second Edition, 1992).

[24] B.L. Finlay, E.D.S. Franco, E.S. Yamada, J.C. Crowley, M. Parsons, J. Augusto, P.C. Muniz, & L.C.L. Silveira. Number and topography of cones, rods and optic nerve axons in New and Old World primates. *Visual Neurosci.* **25** 289–299 (2008). doi:10.1017/S0952523808080371

[25] M.R. Garvie & C. Trenchea. Identification of space-time distributed parameters in the Gierer-Meinhardt reaction-diffusion system. *SIAM J. Appl. Math.* **74** 147–166 (2014) DOI 10.1137/120885784

[26] A. Gierer & H. Meinhardt. A theory of biological pattern formation. *Kybernetik* **12** 30–39 (1972).

[27] C.E. Granger, Q. Yang, H. Song, K. Saito, K. Nozato, L.R. Latchney, B.T. Leonard, M.M. Chung, D.R. Williams, & E.A. Rossi. Human retinal pigment epithelium: In vivo cell morphometry, multispectral autofluorescence, and relation to cone mosaic. *Invest. Ophth. Vis. Sci.* **59** 5705–5716 (2018) https://doi.org/10.1167/iovs.18-24677

[28] C.J. Guérin, D.H. Anderson, R.N. Fariss, & S.K. Fisher. Retinal reattachment of the primate macula. *Invest. Ophth. Vis. Sci.* **30** 1708–1725 (1989).

[29] C.J. Guérin, G.P. Lewis, S.K. Fisher, & D.H. Anderson. Recovery of photoreceptor outer segment length and analysis of membrane assembly rates in regenerating primate photoreceptor outer segments. *Invest. Ophth. Vis. Sci.* **34** 175–183 (1993).

[30] J.C. Horton, A.B. Parker, J.V. Botelho, & J.L. Duncan. Spontaneous regeneration of human photoreceptor outer segments. *Sci. Rep.* **5** 12364 (2015) DOI: 10.1038/srep12364

[31] R. Kafieh, H. Rabbani, F. Hajizadeh, M.D. Abramoff, & M. Sonka. Thickness mapping of eleven retinal layers segmented using the diffusion maps method in normal eyes. *J. Ophthalmol.* **2015** 259123 (2015) https://dx.doi.org/10.1155/2015/259123

[32] H. Kolb, E. Fernandez, & R. Nelson, editors. *Webvision: The Organization of the Retina and Visual System [Internet]*. Salt Lake City (UT): University of Utah Health Sciences Center; 1995 https://www.ncbi.nlm.nih.gov/books/NBK11556

[33] R. Legras, A. Gaudric, & K. Woog. Distribution of cone density, spacing and arrangement in adult healthy retinas with adaptive optics flood illumination. *PLOS ONE* **13** e0191141 (2018).

[34] I.Y.-F. Leung, M.M. Sandstrom, C.L Zucker, M. Neuringer, and D.M. Snodderly. Nutritional manipulation of primate retinas. IV. Effects of n–3 fatty acids, lutein, and zeaxanthin on S-cones and rods in the foveal region. *Exp. Eye Res.* **81** 513–529 (2005) doi:10.1016/j.exer.2005.03.009

[35] T. Léveillard, S. Mohand-Saïd, O. Lorentz, D. Hicks, A.-C. Fintz, E. Clérin, M. Simonutti, V. Forster, N. Cavusoglu, F. Chalmel, P. Dollé, O. Poch, G. Lambrou, & J.A. Sahel. Identification and characterization of rod-derived cone viability factor. *Nat. Genet.* **36** 755–759 (2004).

[36] J. Liu, H. Jung, A. Dubra, & J. Tam. Automated photoreceptor cell identification on nonconfocal adaptive optics images using multiscale circular voting. *Invest. Ophth. Vis. Sci.* **58** 4477–4489 (2017).

[37] T. Liu, H. Jung, J. Liu, M. Droettboom, & J. Tam. Noninvasive near infrared

autofluorescence imaging of retinal pigment epithelial cells in the human retina using adaptive optics. *Biomed. Opt. Express* **8** 4348–4360 (2017).

[38] Z. Liu, O.P. Kocaoglu, & D.T. Miller. 3D imaging of retinal pigment epithelial cells in living human retina. *Invest. Ophth. Vis. Sci.* **56** OCT533–OCT543 (2016) DOI: 10.1167/iovs.16-19106

[39] M. Lombardo, S. Serrao, P. Ducoli, & G. Lombardo. Eccentricity dependent changes of density, spacing and packing arrangement of parafoveal cones. *Ophthal. Physl. Opt.* **33** 516–526 (2013) doi: 10.1111/opo.12053

[40] Y. Lu, T. Son, T.-H. Kim, D. Le., & X. Yao. Virtually structured detection enables super-resolution ophthalmoscopy of rod and cone photoreceptors in human retina. *Quant. Imaging Med. Surg.* **11** 1060–1069 (2021) https://dx.doi.org/10.21037/qims-20-542

[41] G. Maden, A. Cakir, D. Icar, B. Erden, S. Bolukbasi, & M. Elcioglu. The distribution of the photoreceptor outer segment length in a healthy population. *J. Ophthalmol.* **2017** 4641902 (2017) https://doi.org/10.1155/2017/4641902

[42] B.D. Masella, J.J. Hunter, & D.R. Williams. Rod photopigment kinetics after photodisruption of the retinal pigment epithelium. *Invest. Ophth. Vis. Sci.* **55** 7535–7544 (2014) DOI: 10.1167/iovs.13-13796

[43] A. Mehri. Non-extensive distribution of human eye photoreceptors. *J. Theor. Biol.* **419** 305–309 (2017).

[44] M. Menghini, B.J. Lujan, S. Zayit-Soudry, R. Syed, T.C. Porco, K. Bayabo, J. Carroll, A. Roorda, & J.L. Duncan. Correlation of outer nuclear layer thickness with cone density values in patients with retinitis pigmentosa and healthy subjects. *Invest. Ophth. Vis. Sci.* **56** 372–381 (2015) DOI: 10.1167/iovs.14-15521

[45] D. Merino, J.L. Duncan, P. Thiruveedhula, & A. Roorda. Observation of cone and rod photoreceptors in normal subjects and patients using a new generation adaptive optics scanning laser ophthalmoscope. *Biomed. Opt. Express* **2** 2189–2201 (2011).

[46] I.K. Muftuoglu, H.L. Ramkumar, D.-U. Bartsch, A. Meshi, R. Gaber, & W.R. Freeman. Quantitative analysis of the inner retinal layer thickness in age-related macular degeneration using corrected optical coherence tomography segmentation. *Retina* **38** 1478–1484 (2018). doi:10.1097/IAE.0000000000001759.

[47] S. Panda-Jones, J.B. Jonas, & M. Jakobczyk-Zmija. Retinal pigment epithelial cell count, distribution, and correlations in normal human eyes. *Am. J. Ophthalmol.* **121** 181–189 (1996).

[48] A. Reumueller, L. Wassermann, M. Salas, M. Schranz, R. Told, K. Kostolna, W. Drexler, M. Pircher, U. Schmidt-Erfurth, & A. Pollreisz. Three-dimensional assessment of para- and perifoveal photoreceptor densities and the impace of meridians and age in healthy eyes with adaptive-optics optical coherence tomography (AO-OCT). *Opt. Express* **28** 36723–36739 (2020) https://doi.org/10.1364/OE.409076

[49] A. Reumueller, L. Wassermann, M. Salas, M. Schranz, V. Hacker, G. Mylonas, S. Sacu, W. Drexler, M. Pircher, U. Schmidt-Erfurth, & A. Pollreisz. Three-dimensional composition of the photoreceptor cone layers in healthy eyes using adaptive-optics optical coherence tomography (AO-OCT). *PLOS ONE* **16** e0245293 (2021) https://doi.org/10.1371/journal.pone.0245293

[50] P.A. Roberts, Inverse problem reveals conditions for characteristic retinal degeneration patterns in retinitis pigmentosa under the trophic factor hypothesis. *Front. Aging Neurosci.* **14** 765966 (2022).

[51] P.A. Roberts, Mathematical models of retinitis pigmentosa: the trophic factor hypothesis. *J. Theor. Biol.* **534** 110938 (2022).

[52] P.A. Roberts, E.A. Gaffney, P.J. Luthert, A.J.E. Foss, & H.M. Byrne. Mathematical and computational models of the retina in health, development and disease. *Prog. Retin. Eye Res.* **53** 48–69 (2016).

[53] P.A. Roberts, E.A. Gaffney, P.J. Luthert, A.J.E. Foss, & H.M. Byrne. Mathematical models of retinitis pigmentosa: The oxygen toxicity hypothesis. *J. Theor. Biol.* **425** 53–71 (2017).

[54] P.A. Roberts, E.A. Gaffney, J.P. Whiteley, P.J. Luthert, A.J.E. Foss, & H.M. Byrne. Predictive mathematical models for the spread and treatment of hyperoxia-induced photoreceptor degeneration in retinitis pigmentosa. *Invest. Ophth. Vis. Sci.* **59** 1238–1249 (2018).

[55] A. Roorda, Y. Zhang, & J.L. Duncan. High-resolution in vivo imaging of the RPE mosaic in eyes with retinal disease. *Invest. Ophth. Vis. Sci.* **48** 2297–2303 (2007) DOI: 10.1167/iovs.06-1450

[56] B. Sajdak, Y.N. Sulai, C.S. Langlo, G. Luna, S.K. Fisher, D.K. Merriman, & A. Dubra. Noninvasive imaging of the thirteen-lined ground squirrel photoreceptor mosaic. *Visual Neurosci.* **33** e008 (2016) doi: 10.1017/S0952523815000346

[57] L. Sawides, A. de Castro, & S.A. Burns. The organization of the cone photoreceptor mosaic measured in the living human retina. *Vision Res.* **132** 34–44 (2017) http://dx.doi.org/10.1016/j.visres.2016.06.006

[58] D. Scoles, Y.N. Sulai, C.S. Lango, G.A. Fishman, C.A. Curcio, J. Carroll, & A. Dubra. In vivo imaging of human cone photoreceptor inner segments. *Invest. Ophth. Vis. Sci.* **55** 4244–4251 (2014) DOI: 10.1167/iovs.14-14542

[59] S.A. Shoaf, K. Conway, & R.K. Hunt. Application of reaction-diffusion models to cell patterning in *Xenopus* retina. Initiation of patterns and their biological stability. *J. Theor. Biol.* **109** 299–329 (1984).

[60] D.M. Snodderly, M.M. Sandstrom, I.Y.-F. Leung, C.I. Zucker, & M. Neuringer. Retinal pigment epithelial cell distribution in central retina of Rhesus monkeys. *Invest. Ophth. Vis. Sci.* **43** 2815–2818 (2002)

[61] H. Song, T.Y.P. Chui, Z. Zhong, A.E. Elsner, & S.A. Burns. Variation of cone photoreceptor packing density with retinal eccentricity and age. *Invest. Ophth. Vis. Sci.* **52** 7376–7384 (2011).

[62] O. Strauss. The retinal pigment epithelium in visual function. *Physiol. Rev.* **85** 845–881 (2005) doi: 10.1152/physrev.00021.2004

[63] T. Ueda-Consolvo, H. Ozaki, T. Nakamura, T. Oiwake, & A. Hayashi. The association between cone density and visual function in the macula of patients with retinitis pigmentosa. *Graef. Arch. Clin. Exp. Ophthalmol.* **257** 1841–1846 (2019) https://doi.org/10.1007/s00417-019-04385-0

[64] Y. Wang, N. Bensaid, P. Tiruveedhula, J. Ma, S. Ravikumar, & A. Roorda. Human foveal cone photoreceptor topography and its dependence on eye length. *eLife* **8** e47148 (2019) https://doi.org/10.7554/eLife.47148.001

[65] E.M. Wells-Gray, S.S. Choi, A. Bries, & N. Doble. Variation in rod and cone density from the fovea to the mid-periphery in healthy human retinas using adaptive optics scanning laser ophthalmoscopy. *Eye* **30** 1135–1143 (2016) doi.10.1038/eye.2016.107

[66] K.C. Wikler, R.W. Williams, & P. Rakic. Photoreceptor mosaic: Number and distribution of rods and cones in the Rhesus Monkey retina. *J. Comp. Neurol.* **297** 499–508 (1990).

[67] M.A. Wilk, B.M. Wilk, C.S. Lango, R.F. Cooper, & J. Carroll. Evaluating outer segment length as a surrogate measure of peak foveal cone density. *Vision Res.* **130** 57–66 (2017).

[68] F. Wong. Investigating retinitis pigmentosa: a laborator scientist's perspective. *Prog. Retin. Eye Res.* **16** 353–373 (1997).

[69] Z. Xia, H. Chen, & S. Zheng. Thickness of macular inner retinal layers in children with anisometropic amblyopia. *Biomed. Res. Int.* **2020** 6853258 (2020). https://doi.org/10.1155/2020/6853258

[70] Z. Zhang, D. Yang, J. Sang, R. Hou, K. Liu, Z. Li, X. Xie, J.B. Jonas, & N. Wang. Reproducibility of macular, retinal nerve fiber layer, and ONH measurements by OCT in Rhesus monkeys: the Beijing Intracranial and Intraocular Pressure (iCOP) Study. *Invest. Ophth. Vis. Sci.* **53** 4505–4509 (2012).